THE JOURNAL OF PHYSICAL CHEMISTRY A
A JOURNAL OF THE AMERICAN CHEMICAL SOCIETY

pubs.acs.org/JPCA Article

Heavy Particle Impact Vibrational Excitation and Dissociation Processes in CO_2

João Vargas,* Bruno Lopez, and Mário Lino da Silva

Cite This: https://dx.doi.org/10.1021/acs.jpca.0c05677 Read Online

ACCESS | Metrics & More | Article Recommendations

ABSTRACT: A heavy particle impact vibrational excitation and dissociation model for CO_2 is presented. This state-to-state model is based on the forced harmonic oscillator (FHO) theory, which is more accurate than current state-of-the-art kinetic models of CO_2 based on first-order perturbation theory. The first excited triplet state $^3B_2$ of CO_2, including its vibrational structure, is considered in our model, and a more consistent approach to CO_2 dissociation is also proposed. The model is benchmarked against a few academic zero-dimensional (0D) cases and compared to decomposition time measurements in a shock tube. Our model is shown to have reasonable predictive capabilities, and the $CO_2 + O \leftrightarrow CO + O_2$ reaction is found to have a key influence on the dissociation dynamics of CO_2 shocked flows, warranting further theoretical studies. We conclude this study with a discussion on the theoretical improvements that are still required for a more consistent analysis of the vibrational/dissociation dynamics of CO_2.

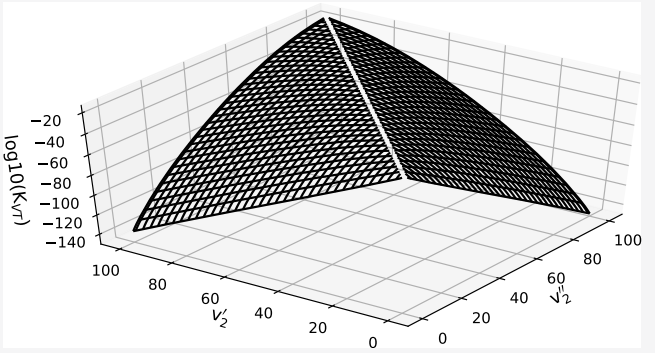

INTRODUCTION

The modeling of CO_2 nonequilibrium vibrational excitation and dissociation/recombination processes is a research topic that has been studied since the mid-20th century. This was initially driven by applications such as CO_2 lasers, combustion, and the design of planetary exploration spacecraft for Venus and Mars, two planets whose atmosphere is mainly composed of CO_2. Since the beginning of the 21st century, the modeling of CO_2 nonequilibrium processes faces renewed interest,[1,2] which is once again driven by applications. While the sizing of planetary exploration spacecraft still remains a major research driver, in the scope of the planning for robotic and crewed exploration of planet Mars, new applications have emerged, such as the low-temperature plasma reforming of CO_2.[3] As a polyatomic molecule with three vibrational degrees of freedom (symmetric stretch *s*, bending *b*, asymmetric stretch *a*), CO_2 exhibits a very complex and at times puzzling array of diverse physical−chemical processes, many of which are only qualitatively known. This means that in parallel with the application-based research, a great deal of theoretical research is also lacking for this molecule.

Recent works in the topic[4−8] make use of rates determined using the Schwartz−Slawsky−Herzfeld (SSH). The SSH theory is a first-order perturbation theory (FOPT), which relies on the scaling of lower-level state-to-state (STS) reaction rate coefficients to obtain higher-lying rates. These may lead to nonphysical values for collision probabilities at high temperatures, which are pervasive in atmospheric entry flows. Additionally, SSH models are limited to single quantum jumps. An alternative to the Schwartz−Slawsky−Herzfeld (SSH) theory would be to apply more accurate trajectory methods (quasi-classical or quantum) over proposed potential energy surfaces (PES) to compute rovibrational energy exchange probabilities. However, PES methods have yet to be applied to large scales and have fallen short of a description up to the dissociation limit of CO_2 due to the inherent computational cost of such sophisticated methods. Increased complexity is still not a realistic option. Instead, a more sophisticated modeling of CO_2 kinetics is still desirable. As such, we propose using the forced harmonic oscillator (FHO) theory to model CO_2 vibrational state-to-state kinetics. The FHO framework was proposed by Treanor in 1965,[9] which also showed that a semiclassical method, based on the same foundations as SSH, could achieve the correct asymptotic behavior predicted by quantum calculations for the case of molecule colliding with an atom. A bi-molecular collision model was later proposed by Zelechow et al.[10] Later developments were brought in the 1990s and early 2000s[11−14] being used in the later 2000s to create a database for Earth atmospheric entries.[15] Since the FHO theory

Received: June 22, 2020
Revised: December 16, 2020

is the extension to higher-order terms of the same kinetic theory the SSH first-order approximation is based on, it maintains an affordable computational budget while keeping the results within the physical limits. Additionally, a more physically consistent treatment of dissociation is achieved by acknowledging the different pathways to CO_2 decomposition, including the enhancement of this process in the presence of O atoms. Coupled with a more adequate treatment of these dissociation pathways, this presents a step up from current vibrational state-to-state kinetic models of CO_2.

This work will be structured as follows: in the Theory section, the theoretical framework of this work will be presented, covering the governing equations, the determination of the manifold of levels, the interactions between singlet and triplet states of CO_2, the calibration with experimental data, the CO and O thermochemistry that was added to the model, and culminating with a brief discussion of the models underlying assumptions and flaws. The Results section will discuss some aspects of the state-specific kinetic data set produced in this work and will present some theoretical test cases for a dissociating and a recombining pure CO_2 flow. A further comparison of decomposition times is carried out against available shock-tube experiments. The Discussion section discusses the major findings of our work, highlighting the importance of the key $CO_2 + O \leftrightarrow CO + O_2$ reaction and discussing the large uncertainty that exists for this reaction at lower temperatures. Possible improvements to the model are discussed, including the influence of radiative losses, and possible strategies for reducing the computational overhead of the rates dataset, which remains intractable for complex multidimensional applications, having over 20 000 state-specific rates.

THEORY

In this section, we describe our theoretical methods and models for determining the vibrational state-to-state rates of CO_2. Firstly the methods for determining the energy levels manifold are discussed, followed by the potential energy surface (PES) crossings between ground-state and electronically excited CO_2. A detailed description of the forced harmonic oscillator (FHO) is passed over in favor of a more qualitative description of the types of reactions this theory is applied to, followed by a brief justification of the use and description of the Rosen−Zener theory for spin-forbidden interactions. The addition of macroscopic chemistry mechanisms to the kinetic scheme is performed on a step-by-step approach culminating with the addition of the CO thermochemistry of Cruden et al.[16] and a recap of the full data set. Finally, a brief discussion on the flaws and limitations of this model, such as the segregation of the CO_2 vibrational modes, merging of the (v_2,l_2) levels in a single v_2 level, neglecting low-temperature effects, neglecting collisional partners other than CO_2 is carried out. A more in-depth discussion on the possible venues for raising such limitations is carried out in the Discussion section.

CO_2 Molecule. CO_2 is a linear triatomic molecule. It has three vibrational modes, symmetric stretch that corresponds to the equal stretch of the C−O bonds in the molecule, and is usually denoted as v_1, *s*, or *ss*. The bending mode corresponds to the deformation of the linearity of the molecule and is usually denoted as v_2, *b*, or *be*. The bending mode is considered doubly degenerate when there is vibrational angular momentum present ($l_2 > 0$). The third and final mode corresponds to the compression of a C−O bond and the stretch of the other C−O mode, the so-called asymmetric stretch that is usually denoted as v_3, *a*, or *as*. A vibrational level of CO_2 might be annotated as $v_1v_2v_3$ or $v_1v_2^{l_2}v_3$ when the vibrational angular momentum number is specified. Many works also use an additional assignment number *r*, the so-called ranking number. It is used when authors prefer to fix $v_2 = l_2$, and provides a convenient way to identify vibrational levels that may be grouped by Fermi resonance. In this work, we will not consider the l_2 structure of bending levels and will assume that $v_2 = l_2$ instead of the possible range of $l_2 = v_2, v_2 - 2, v_2 - 4, ..., 1$ or 0. As such, all bending levels have a degeneracy of 2 instead of $g = v_2 + 1$. Additionally, using $g = v_2 + 1$ would be assuming that the average energy for v_2 levels (considering the possible l_2 manifold) would be at $v_2 = l_2$, which is significantly higher than the actual average at high v_2. Both models were compared against each other, and no major differences in the computed macroscopic and microscopic quantities were detected.

On the Fermi Resonance Question. Fermi resonance is an effect in which vibrational levels with the same molecular symmetry and a small energy gap are shifted in the spectrum, with a bigger energy gap and with line intensities different from those expected. This is usually interpreted as a coupling between the symmetric and bending modes of CO_2.[17] This phenomenon is often invoked to justify the use of a single temperature to characterize the symmetric and bending modes. In this work, no a priori coupling between the symmetric and bending modes is assumed. Since the included bending levels are considered to be $v_2 = l_2$, there are no symmetric levels with the same molecular symmetry and therefore no mode coupling is considered in this work. Furthermore, it cannot be reasonably assumed that the small energy gap condition for Fermi resonance to occur is maintained higher in the vibrational ladder where anharmonicity effects lead to a wider gap between the "would-be" resonant states. As such, only "accidental" resonances may a-priori occur between higher-lying levels, which ties into the concept of vibrational chaos. It is also worth mentioning that Fermi resonances in the level energies do not always translate to equiprobable level populations for the resonant states[18−21] and that the fitting of high-resolution infrared Fourier transform (FTIR) spectra in the 4.3 μm region is insensitive to the v_1 and v_2 level populations, which means that the error bars in the fits allow for a great latitude of interpretation of the level populations for symmetric and bending states, which may be considered with separate temperatures ($T_{v_1} \neq T_{v_2}$)[22] or with equivalent temperatures ($T_{v_1} = T_{v_2}$)[23] indistinguishably (private communications).

Level Energies. The first step in the generation of new reaction rates is to determine a manifold of level energies. In this work, this is performed for the ground state and the electronically excited state $^3B_2$. We start with the ground state. Since there are no ground-state potential energy surfaces (PES) that are accurate up to the dissociation energy of CO_2, the asymptotic limits of dissociation must first be established. These must be different for each mode as each breaks apart in a different configuration. The dissociation energy may be obtained against the balance of the enthalpies of formation for the products of dissociation. These are as follows:

- Symmetric stretch: $CO_2(X^1\Sigma) + 18.53\ eV \rightarrow C(^3P) + O(^3P) + O(^1D)$,
- Bending: $CO_2(X^1\Sigma) + 11.45\ eV \rightarrow C(^3P) + O_2(X^3\Sigma)$,
- Asymmetric stretch: $CO_2(X^1\Sigma) + 7.42\ eV \rightarrow CO(X^1\Sigma) + O(^1D)$.

https://dx.doi.org/10.1021/acs.jpca.0c05677
J. Phys. Chem. A XXXX, XXX, XXX−XXX

Having the asymptotic behavior of each mode allows the extension of a PES to the near-dissociation limit, and thus, a well-behaved one-dimensional (1D) potential curve for each mode is obtained. This approach is the known Rydberg−Klein−Rees (RKR) method, which is detailed in ref 24. Upon obtaining a well-behaved potential curve, the radial Schrödinger's equation may be solved and a manifold of levels can be determined. The NASA-Ames-2 PES by Huang et al.[25] (kindly shared by Dr. Huang) is used up to 25 500 cm^{-1} and extended to the respective dissociation limit in the long range for the symmetric and asymmetric stretch modes by Hulburt[26] and Rydberg[24] potentials, respectively. In the short range, the potential is extended by a repulsive curve of the form (a/x^b). Thus, the 1D potentials of the symmetric and asymmetric stretch modes are obtained and reported in Figures 1 and 2, respectively. The

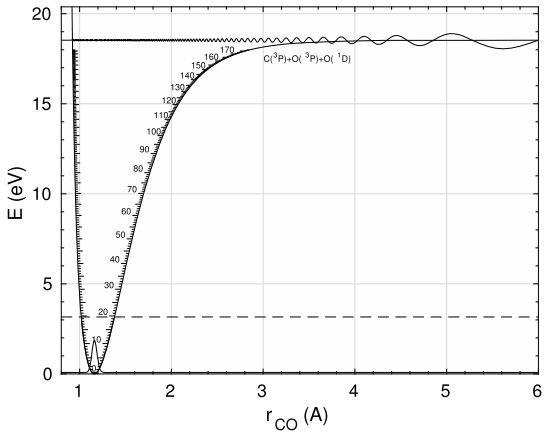

Figure 1. Symmetric 1D potential of the CO_2 ground state with extrapolation to correct the asymptotic limit of potential by the RKR method. The extrapolation is done above the dashed line, below which the curve is given by the NASA-Ames-2 PES.

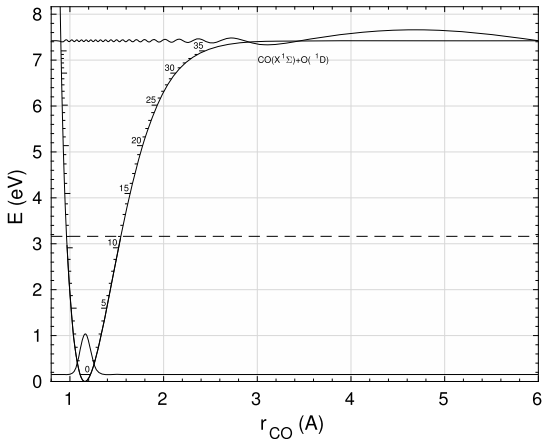

Figure 2. Asymmetric 1D potential of the CO_2 ground state with extrapolation to correct the asymptotic limit of potential by the RKR method. The extrapolation is done above the dashed line, below which the curve is given by the NASA-Ames-2 PES.

dotted line in each figure represents the limit to which the NASA-Ames-2 PES is used, above which the potentials are extrapolated. The eigenvalues obtained from the radial Schrödinger's equation are also plotted along the potential curve. A full line at 18.53 and 7.42 eV represents the asymptotic limit for the potential curve of each mode, along with the first and last bound solution of Schrödinger's equation. The bending mode requires a different treatment. The symmetry of the bending mode potential excludes the possibility of using the same treatment described above as there is no expectation for the shape of the potential near the asymptotic limit. Furthermore, it is of no benefit to model such extreme states close to the dissociation limit of "pure" bending of the molecule. Nevertheless, due to the symmetry of the bending mode, the potential may be fitted to a polynomial expression $ax^2 + bx^4$ as described in ref 27.[a] As for the energy levels, and once more acknowledging the symmetry of the potential, these may be extrapolated from a polynomial expression with a greater degree of confidence. In this work, the Chedin polynomial fit[28] is used for this purpose. Figure 3 shows the symmetry of the bending

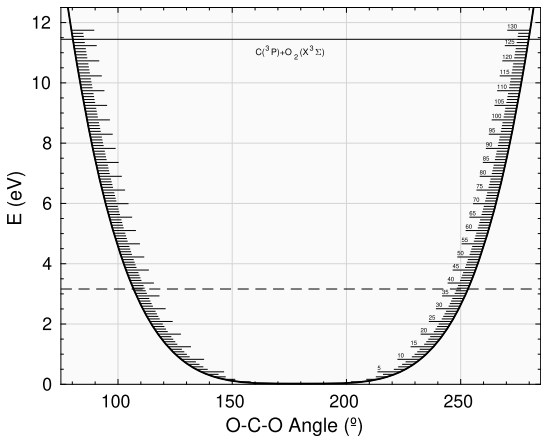

Figure 3. Bending angular potential of the CO_2 ground state. Above the dashed line, extrapolation of the potential is performed by the expression $ax^2 + bx^4$, below which the curve is given by the NASA-Ames-2 PES.

mode along with the energy levels obtained from the Chedin fit. In the same figure, the dashed line represents the threshold above which the potential is extrapolated from the NASA-Ames-2 PES. A solid line represents the asymptotic limit, which cannot be captured by the extrapolation of the employed $ax^2 + bx^4$ polynomial.

Electronically excited CO_2 in the $^3B_2$ state is a bent molecule in its equilibrium configuration with the same vibrational modes as the ground-state CO_2. Although there are some available PES for this excited state, not having the symmetry of a linear molecule precludes the use of the same methods as in the fundamental state. Solutions to Schrödinger's equation could possibly be found but the assignment of each solution to a state would be a complex endeavor, which requires a work of its own. Instead, we will use the values found and assigned in the work of Grebenshchikov.[29] These may be used to fit a polynomial based on the same expression as the Chedin fit.[28] The resulting polynomial takes the form

$$E(v_1, v_2, v_3) = \sum_{i=1,2,3} \omega_i v_i + \sum_{i=1,2,3} x_{ii} v_i^2 + x_{12} v_1 v_2 + x_{13} v_1 v_3 + x_{23} v_2 v_3 \quad (1)$$

The coefficients found through this polynomial fit are reported in Table 1. Figure 4 presents the levels found by fitting the values in ref 29 to eq 1. The circles with an inscribed cross are the values found in ref 29 and the other circles are energy levels found from extrapolating the fit. The fine dotted line labeled MSX1 is the

https://dx.doi.org/10.1021/acs.jpca.0c05677
J. Phys. Chem. A XXXX, XXX, XXX−XXX

Table 1. Coefficients Obtained from Fitting the Expression in Equation 1 to the Energy Levels Found in Ref 29 in Units of cm^{-1}

ω_1	ω_2	ω_3	x_{11}	x_{22}
1.387×10^3	6.031×10^2	1.092×10^3	-8.254×10^0	2.311×10^{-1}
x_{33}	x_{12}	x_{13}	x_{23}	
1.501×10^0	-1.358×10^1	-6.422×10^1	-1.808×10^1	

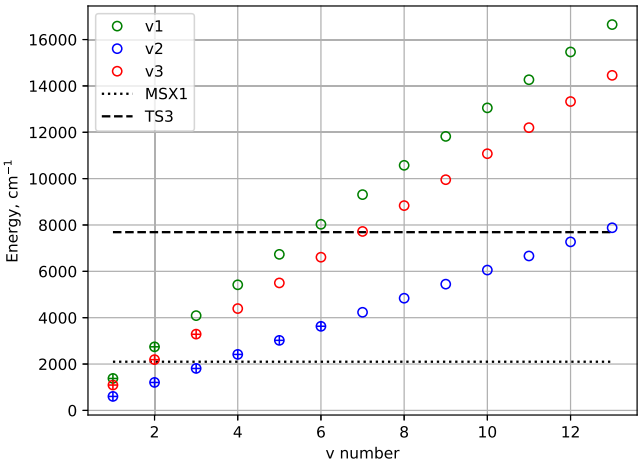

Figure 4. Manifold of vibrational levels of $CO_2(^3B_2)$ used in this work. These levels were determined with equation 1 and with the coefficients in Table 1. MSX1 refers to the seam of crossing energy of the $CO_2(^3B_2)$ with the ground state, and TS3 refers to the dissociation energy of $CO_2(^3B_2)$.

seam of crossing between the ground state of CO_2 and the $^3B_2$ state. The line labeled as TS3 is the dissociation energy of the $^3B_2$ state. Usually, the spacing of levels will be lowered as the dissociation limit is approached. This is not the case in the asymmetric stretch mode of the $^3B_2$ state as the extrapolation of a polynomial expression does not allow replicating this behavior. However, as a first approximation, it is a reasonable enough estimation. The line labeled as TS3 is the dissociation limit of the $^3B_2$ state. We assume that as in the case of the ground state the asymptotic limit for each mode will be different and as such the symmetric and bending modes are not bound by TS3.

This concludes the determination of the level manifold used in this work. The levels considered for this work are summarized in Table 2. The number of levels in the v_3 mode for both

Table 2. Manifold of Levels for Each Vibrational and Electronic Mode of CO_2

CO_2	v_1	v_2	v_3
$X^1\Sigma$	59	100	41
$^3B_2$	12	25	6

electronic states is fixed since dissociation occurs through this mode. A v_3 level above the dissociation limit is considered to be quasi-bound (q.b.), meaning a level corresponding to a solution of Schrödinger's equation with a closed wave function on one side and an open one on the other. These states are considered to be inherently unstable and dissociate with probability 1.[11,13−15] The number of levels in the other modes may differ. We have elected to use 59 and 100 levels since these correspond to the same energy chosen arbitrarily, roughly ≈9 eV. No study was conducted to verify the sensitivity of the number of levels in the other modes. However, it was verified that using a smaller amount of levels in the ground state would lead to greater numerical instability in the code. With the levels included in Table 2 and the ground state of each electronic level, there is a total of 245 vibrational levels in the model.

PES Crossings. In this work, we aim to account for the different pathways to dissociation of CO_2. For this, the configuration of the interactions between the ground and electronically excited states of CO_2 needs to be defined. The work of Hwang and Mebel[30] provides a basis for the configuration of these interactions. There are two seams of crossings between the ground and $^3B_2$ states of CO_2. The first takes place at approximately 4.99 eV when the CO_2 molecule is bent close to the equilibrium configuration of the $^3B_2$ state. The exact configuration of the crossing will depend on the calculation method used. Looking at the range of values proposed in ref 30, we define an approximate region for the exact configuration, between 1.22−1.30 Å and 105.0−110.4°, assuming the C−O bonds to be the same length. This region is plotted in Figure 5 as

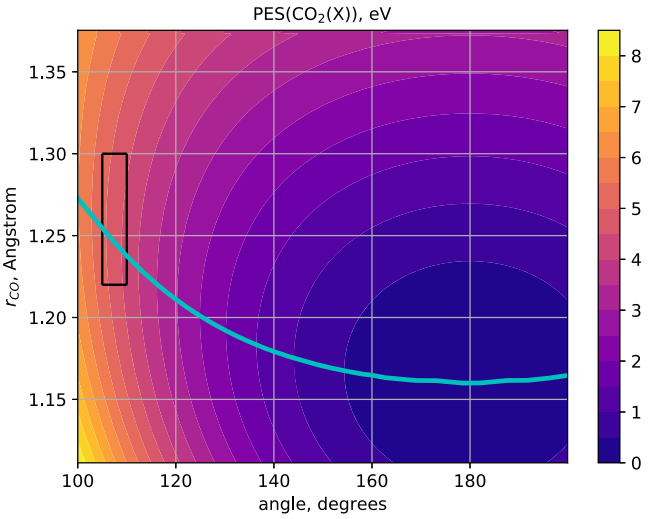

Figure 5. Color map of the PES of the ground state of CO_2 with $r_{CO1} = r_{CO2}$. The cyan line that crosses the color map is the equilibrium r_{CO} distance given a specific angle. The black box on the left side of the figure is the probable configuration space for the crossing between the CO_2 ground and triplet states.

a black box. Figure 5 also presents a three-dimensional (3D) color map for the PES of the ground state of CO_2 considering both C−O bonds at the same length and varying the angle between them. The cyan line in the aforementioned figure is the position of the potential minimum at each angle. The cyan line intersects the region where the exact configuration of the crossing is most likely to be. This indicates that the crossing may occur purely through the ground state with v_2 excitation, as this mode will play the main role interacting with the $^3B_2$ excited state. Only a few vibrational levels close to the crossing will interact with the bending levels of the ground state. The interacting $^3B_2$ levels have been defined as those within 2000 cm^{-1} of the crossing (MSX1). These coincide with the levels listed in the work of Grebenshchikov.[29]

https://dx.doi.org/10.1021/acs.jpca.0c05677
J. Phys. Chem. A XXXX, XXX, XXX−XXX

The second crossing takes place at 5.85 eV in a linear configuration of ground-state CO_2 but with the bonds at very different lengths. In this crossing, the determined configuration in ref 30 has one bond length at approximately 1.9 Å and the other bond at 1.3 Å. This suggests that the mode, which interacts the most in this crossing, is the asymmetric stretch, v_3. The excited state in this crossing is in a repulsive configuration and excitation to this state will lead to immediate dissociation. As we do not have the functional form for the triplet state, there is no possibility to compute the energy levels of the quasi-bound states. As such, we assume there is a level at the energy of the crossing of 5.85 eV to which the v_3 levels of the ground state of CO_2 will dissociate to.

We have now defined which levels are interacting in which crossings. The theory that is usually applied in vibrational state-to-state collisions is the Landau−Zener theory. Since these crossings are singlet−triplet interactions, this theory cannot be straightforwardly applied in this case. The next subsection discusses some of these details. There are other singlet and triplet electronically excited states of CO_2 in a configuration alike to the $^3B_2$ level, which was discussed in this section. These other states are not considered in this work due to the scarcity of published data on crossings between the ground state and other electronically excited states of CO_2.

Vibration−Translation Processes. Here, we summarize the key equations for this theory and its extension to triatomic molecules such as CO_2. The inner details of the FHO theory and its different generalizations are not described here and may be consulted in refs 15 and 31.

The FHO model computes vibrational−translational (VT) energy exchanges

$$CO_2(i) + M \leftrightarrow CO_2(f) + M \tag{2}$$

where i and f are the vibrational levels for the same mode and M is a generic collision partner. In these reactions, the electronic state can be the X or $^3B_2$. The corresponding FHO transition probability is[9,32]

$$P(i\rightarrow f,\ \varepsilon) = i!f!\varepsilon^{i+f}\ \exp(-\varepsilon)\left|\sum_{r=0}^{n}\frac{(-1)^r}{r!(i-r)!(f-r)!\varepsilon^r}\right|^2 \tag{3}$$

with $n = \min(i, f)$. ε is related to the first-order perturbation theory (FOPT) transition probability $\varepsilon = P_{\mathrm{FOPT}}(1 \rightarrow 0)$.

For transitions involving larger vibrational number changes and at higher-vibrational numbers, it is no longer possible to accurately compute transition probabilities using exact FHO factorial expressions. When such a computation is not possible, these are instead replaced by the approximations suggested by Nikitin and Osipov[33] that make use of Bessel functions. Details of these approximations are found in refs 15 and 31. Dissociation (vibration−dissociation (VD) reactions) may occur through the asymmetric stretch mode when the level in the products of the reaction is quasi-bound (q.b.)

$$CO_2(v_3) + M \leftrightarrow CO_2(\text{q. b. }) + M \overset{P=1}{\longleftrightarrow} CO + O + M \tag{4}$$

where the dissociation products are $CO(X^1\Sigma)$ and $O(^1D)$ in case the reactant is the ground state and $CO(X^1\Sigma)$ and $O(^3P)$ in case the reactant is the $^3B_2$ state. Dissociation is considered to be the only possible outcome for a quasi-bound state, and the recombination reaction is computed through detailed balance. It is worthwhile to examine the different ways to model dissociation using FHO.

Adamovich et al.[11] were the first to propose an approach for dissociation under the FHO framework. Therein, dissociation was assumed as a two-step process, including a jump from an initial level i to the last bound state of a molecule v_{diss}, followed by a decay to dissociation from the last bound state with $P_{\mathrm{decay}} \sim 1$. The authors note that this is an approximation not valid for high i and should only be applied to situations where dissociation occurs primarily through the lower vibrational levels. A more refined approach to dissociation under the FHO framework was then proposed by Macheret and Adamovich,[14] wherein a Morse potential is calibrated against the lower vibrational levels yielding a potential that may be used to compute bound levels above the experimental dissociation energy. Although the energy values for these levels are less than accurate, the FHO theory may still be applied to the calculations of transitions between the levels below the dissociation threshold and the fictitious levels above the dissociation threshold. Lino da Silva et al. then proposed[24,34−38] another approach to dissociation, wherein a more realistic potential was obtained from other works (direct-potential fits, e.g., ref 39) or recalculated through the RKR method.[24] The radial Schrödinger's equation is then solved over such a potential, yielding a set of energy levels and wave functions bound within the potential curve repulsive and near-dissociation limits (so-called bound levels), but also energies and wave functions above the dissociation limit, only bound by the repulsive side of the potential (unbound/quasi-bound level). These levels up to a certain threshold in energy (above the dissociation limit) are included in the overall calculations for all of the possible multiquantum transitions. Then, all of the transitions between an initial bound quantum number i and a final level f with $f > v_{\mathrm{diss}}$ are summed and considered to be a global dissociation rate $K_{i\rightarrow\mathrm{diss}}$. This approach was applied in a past work[37] that aimed at producing a set of multiquantum vibrational rates for all of the five neutral species of air (N_2, O_2, NO, N, and O), and the obtained state-specific dissociation rates were summed into an equilibrium rate, assuming a Boltzmann distribution for the vibrational energy levels. Then, these dissociation rates were compared against dissociation rates from five different popular chemistry sets for air and were found to fall within the upper and lower bounds for these rate data sets.

This has allowed the authors to have confidence in applying this same approach to the dissociation of CO_2. Within this framework, the overall probability for a level v_3 to dissociate is the sum of all possible $CO_2(v_3) + M \leftrightarrow CO_2(\text{q.b.}) + M$ processes. The sum may be carried out over an increasing number of quasi-bound states (each with higher energy); however, the higher the difference in quanta, the higher the threshold energy for the transition will be, with the resulting rate being lower at a given temperature. Accordingly, the dissociation rate calculation must be truncated at some preset temperature (in this work, 100 000 K), which ensures that if a process with a certain Δv is negligible, processes with higher Δv will also be negligible. As such, the sum of dissociation rates will tend to the same global dissociation rate for each level. The criterion for the quantum level threshold is not obtainable analytically but instead numerically since the spacing of the calculated unbound levels above the dissociation threshold will still depend on the behavior of the repulsive part for each species potential level. Here, we have verified that including more than 38 levels above dissociation in the case of the CO_2 ground-state asymmetric

https://dx.doi.org/10.1021/acs.jpca.0c05677
J. Phys. Chem. A XXXX, XXX, XXX−XXX

yielded negligible differences in the calculated thermal dissociation rate. For the case of the CO_2 triplet state, in the absence of reliable analytic potential surfaces from the literature, the asymmetric stretch levels above dissociation were found through fitting a polynomial to the lower vibrational levels; therefore, this approach could be considered as akin to the treatment in ref 14, with the criterion for cutoff different from the ground state. In this case, a cutoff of seven vibrational levels above the dissociation limit was considered.

A VT reaction may also occur when the initial and final levels are not in the same mode (intermode vibration−translation, IVT). In that case, the VT reaction is considered to be two VT reactions and the total probability is considered to be the product of these two collision probabilities

$$CO_2(i) + M \leftrightarrow CO_2(0) + M \leftrightarrow CO_2(f) + M \quad (5)$$

where $CO_2(0)$ is the fundamental vibrational state of either the ground electronic state or the $^3B_2$ state. We note that this approximation will lead to vanishingly small transition probabilities at higher v's.[b] This might not be necessarily the case since many accidental resonances may occur for these higher levels, which means our method may be underestimating IVT processes in this specific case. Approaches to address this shortcoming will be discussed more ahead in the Discussion section. Finally, a vibrational−vibrational (VV) reaction may also be modeled. In our model, we have chosen to only account for near-resonant VV processes, with one molecule gaining a vibrational quanta and the other losing one quanta. Further nonresonant vibration−vibration−translation (VVT) processes are considered negligible in a first approach since accounting for them would considerably burden our computational model. The VVT reactions we chose to model are of the form

$$CO_2(v) + CO_2(v) \leftrightarrow CO_2(v+1) + CO_2(v-1) \quad (6)$$

The FHO transition probability for a VVT reaction in the general case is[10]

$$P(i_1, i_2 \rightarrow f_1, f_2, \varepsilon, \rho) = \left| \sum_{g=1}^{n} (-1)^{(i_{12}-g+1)} C_{g,i_2+1}^{i_{12}} C_{g,f_2+1}^{f_{12}} \varepsilon^{(i_{12}+f_{12}-2g+2)/2} e^{-\varepsilon/2} \sqrt{(i_{12}-g+1)!(f_{12}-g+1)!}\, e^{-i(f_{12}-g+1)\rho} \sum_{l=0}^{n-g} \frac{(-1)^l}{(i_{12}-g+1-l)!(f_{12}-g+1-l)!l!\varepsilon^l} \right|^2 \quad (7)$$

with $i_{12} = i_1 + i_2, f_{12} = f_1 + f_2$ and $n = \min(i_1 + i_2 + 1, f_1 + f_2 + 1)$. In the above equation, ε has the same definition as in eq 3, ρ is also related to the FOPT transition probability $\rho = [4 \cdot P_{FOPT}(1, 0 \rightarrow 0, 1)]^{1/2}$, and C_{ij}^k is a transformation matrix.[15] In these reactions, a residual amount of energy is transferred to the translational movement of the molecules due to the anharmonicity of the vibrational ladder. Equation 7 can then be used in the case of the aforementioned VVT transition in eq 6.

Certain parameters in the model must be adjusted such that experimental measurements may be effectively reproduced by the calculations. As such, a so-called semiempirical adjustment of collision parameters takes place. Most notably, the intermolecular potential, which is taken as a Morse potential with shape $V = E_m\{1 - \exp[-\alpha(r - r_{eq})]\}^2$, and the steric factors, which are corrective factors to account for the isotropy of collisions when these are computed in a 1D framework, will be adjusted such that calculations will match experimental rate coefficient measurements in the best possible way. The expressions for ε and ρ are given by Cottrell[40] and Zelechow[10]

$$\varepsilon = \frac{8\pi^3\omega(\tilde{m}^2/\mu)\gamma^2}{\alpha^2 h} \frac{\cosh^2\left[\frac{(1+\phi)\pi\omega}{\alpha\bar{v}}\right]}{\sinh^2\left(\frac{2\pi\omega}{\alpha\bar{v}}\right)}$$

$$\phi = (2/\pi)\tan^{-1}\sqrt{(2E_m/\tilde{m}\bar{v}^2)} \quad (8)$$

$$\rho = 2(\tilde{m}^2/\mu)\gamma^2\alpha\bar{v}/\omega \quad (9)$$

In the expressions above, $\tilde{m}$ is the reduced mass of the colliding molecules, $\bar{v}$ is the symmetric collision velocity $(v_i + v_f)/2$, and ω is the average frequency of the collision as introduced in ref 11

$$\omega = \begin{cases} |E_i - E_f|/(i-f), & i \neq f \\ |E_{i+1} - E_i|, & i = f \end{cases} \quad (10)$$

The corresponding mass parameters have been obtained for the three motions of CO_2 (symmetric stretch, asymmetric stretch, and bending; see Figure 6). These are reported in Table 3. The $^3B_2$ state is bent in its equilibrium configuration, but the same parameters in Table 3 are considered valid for the time being.

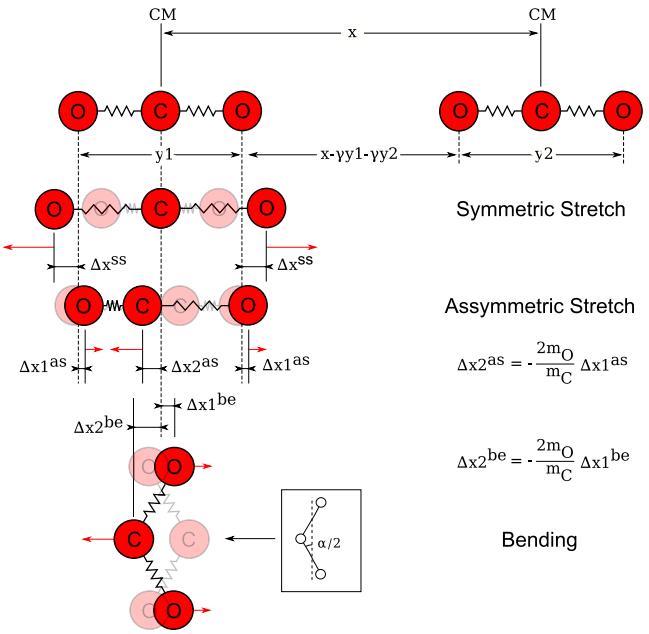

Figure 6. CO_2 mass coordinates for the symmetric stretch, asymmetric stretch, and bending modes.

Table 4 presents the semiempirical coefficients obtained in the adjustment. The first two columns are for pure VT and VVT

Table 3. Mass Parameters for the Three Vibrational Modes of CO_2

osc. mode	reduced mass μ	mass param. γ
sym. stretch	m_O	1/2
asym. stretch	$\frac{m_C m_O}{m_C + 2m_O}$	1/2
bending	$\frac{m_C m_O}{2(2m_O + m_C)}$	1/2

https://dx.doi.org/10.1021/acs.jpca.0c05677
J. Phys. Chem. A XXXX, XXX, XXX−XXX

Table 4. Collision Parameters Used in the FHO Rate Calculation Processes

	$VT_{s,b,a}$	$VVT_{s,b,a}$	$IVT_{s,b}$	$IVT_{s,a}$	$IVT_{b,a}$
S_{VT} (10^{-4})	6		2	1	6
S_{VVT} (10^{-3})		6.5			
α (Å^{-1})	4.3	4.3	3.0	4.3	4.3
E (K)	650	650	300	650	650

reactions as described in eqs 2 and 6. The last three columns are specific for IVT reactions such as those in eq 5 and correspond to legacy calibrations against experimental rates. These coefficients have not been updated from a previous calculation of IVT transitions[31] since there was no noticeable improvement without incurring into unplausible values for the space for the parameters. Additionally, the obtained rates will be dominated by the Δv between the initial and final vibrational numbers for the different modes, corresponding to a rapid decline in transition probabilities as the vibrational number is increased. All experimental measurements are made for the ground state of CO_2, and it is assumed they are the same for $CO_2(^3B_2)$ since there is no experimental data available for calibrating the FHO model. Some of the adjustment results are presented in Figure 7 where examples of the VT and VVT reaction rates found in the literature may be recovered after adjusting the semiempirical coefficients accordingly. More examples can be found in ref 31.

Vibrational−Electronic Processes. Earlier works[41,42] studied the crossings mentioned in the PES Crossings section. Therein, spin-forbidden vibrational−electronic (VE) interactions were analysed within the Landau−Zener theory. In these works, the authors proposed to use the off-diagonal terms of the Hamiltonian of the system, which is nonzero for the singlet−triplet interaction, for obtaining the probability of the crossing. The difficulty would then lie in determining the off-diagonal term, which coincides with the spin−orbit coupling term. Though this is mathematically sound, the Landau−Zener theory was developed assuming a constant off-diagonal term.[43] The Rosen−Zener theory is better adapted to spin-forbidden interactions, although we have not verified the range of applicability for this theory in this case. The preference of this theory over the Landau−Zener theory can be justified thus: "The Rosen−Zener model, [...] can be associated with the one-dimensional motion of a system featuring the exponential off-diagonal coupling between the zero-order states of constant spacing [...]." as can be read in the review of Nikitin.[43] It continues: "In a way, this model [Rosen−Zener] is the opposite to the avoided crossing Landau−Zener model, for which the spacing between the zero order states features the crossing while the off-diagonal term is constant". In other words, the crossing of singlet−triplet interactions is described by the off-diagonal terms in the Hamiltonian of the system. The Landau−Zener theory assumes a description of the crossing contained in the diagonal terms, while the Rosen−Zener theory assumes this description to be featured in the off-diagonal term. This is the case in the crossings that are dealt with in this work, and thus, the use of the Rosen−Zener theory is justified.

The Rosen−Zener probability may be written as a function of velocity v

$$P(v) = \left[1 + \exp\left(\frac{\pi \Delta E}{\hbar \alpha v}\right)\right]^{-1} \tag{11}$$

The probability is dependent on the difference in energy of the interacting levels ΔE and the repulsive term of the interaction potential α. With the current expression and with no data to calibrate the rate coefficients for these kinds of reactions, we are forced to use the values as they are calculated. The expression above tends to 1/2 in the high-velocity limit. In the high-temperature regimes, this might lead to a somewhat higher than expected rate coefficient, comparable (but still lower) to the collisional rate coefficient. Thus, the interaction between the singlet ground state of CO_2 and the triplet $^3B_2$ state of CO_2 is taken care of. A schematic of the overall model discussed in this work is presented in Figure 8. The ground state is labeled as X, the excited triplet state as B, and their respective vibrational modes are presented. The arrows outline all the possible interactions within our model.

For the sake of simplicity, our model does not include the effect of Franck−Condon (F.C.) factors on the different calculated VE rates. Although no previous studies exist for the case of collisional processes with polyatomic species such as CO_2, there is a fair amount of experimental studies for the case of diatomic molecules with contradictory findings. Some experimental studies show good correlation with F.C. factors, such as Bondybey et al.,[44] Katayama et al.,[45−47] and Dentamaro et al.[48] Other works instead evidence weak to no correlation between

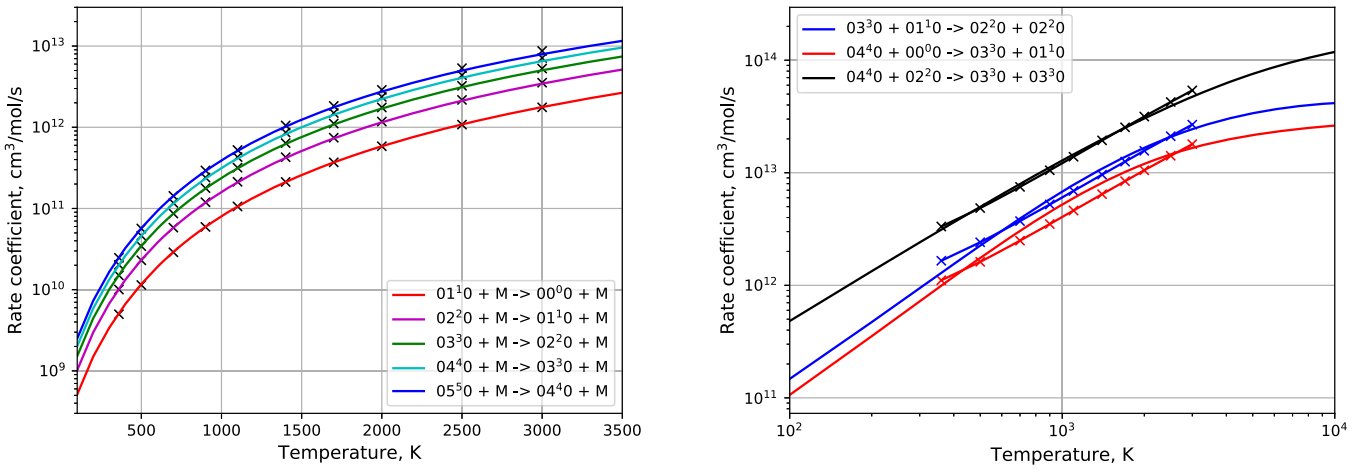

Figure 7. Examples of adjustment of FHO computed rates to SSH published VT rates (left) and experimentally determined VVT rates (right). The used collision parameters may be found in Table 4. More examples of these adjustments are found in ref 31.

https://dx.doi.org/10.1021/acs.jpca.0c05677
J. Phys. Chem. A XXXX, XXX, XXX−XXX

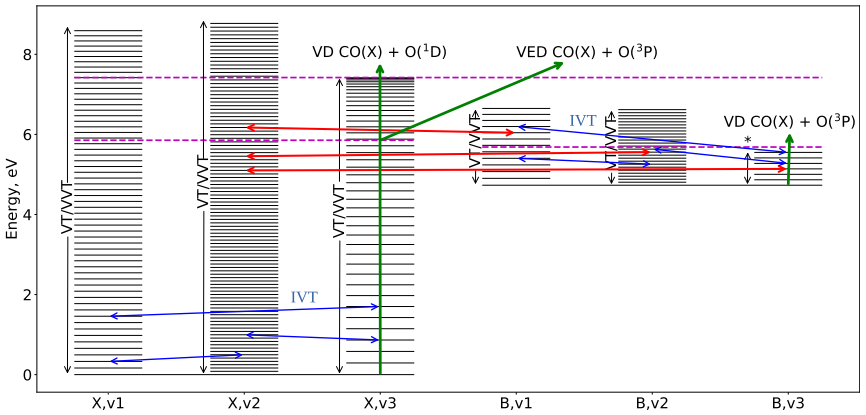

Figure 8. Schematic of the kinetic model with included levels and types of interactions between levels. Dissociation reactions indicate the products of dissociation, and the dashed lines represent the crossings or dissociation limits for certain configurations of CO_2. The exact spacings between adjacent vibrational levels are reported in the figure.

measured VE rates and F.C. factors, such as Bachmann et al.,[49] Jihua et al.,[50] and Piper.[51] Still, the impact of the F.C. factors on the overall rates may be assessed. Since these are typically within the 10^{-1}−10^{-3} interval, the inclusion or exclusion of the F.C. factors may be approximately tested considering a zero-dimensional (0D) simulation of a pure CO_2 shock at 3.69 km/s, 1 Torr and 300 K as in Figure 9 where the evolution of the

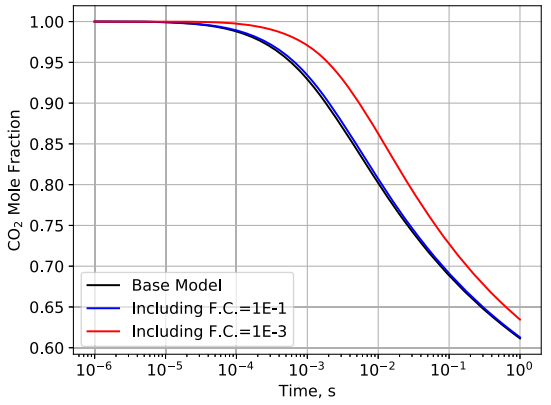

Figure 9. Post-shock CO_2 mole fraction from a 3.690 km/s shock in pure CO_2 at 1 Torr and 300 K using the model described so far and schematically reproduced in Figure 8 (black) and assuming F.C. factors equal to 10^{-1} (blue) and 10^{-3} (red).

CO_2 molar fraction after the shock is shown considering no F.C. factors (black) and accounting them as a corrective factor of 10^{-1} (blue) and 10^{-3} (red). Considering the lower value for the F.C. factors delays dissociation considerably. This will have an impact on the creation of free oxygen atoms, which may then impact the decomposition of CO_2.[52]

Macroscopic Chemistry. At this point, simulations were conducted to test if the model with its current dissociation pathways is consistent with typical dissociation times and degrees for CO_2. A 1D shock wave at 3.690 km/s was simulated passing a CO_2 gas at 1 Torr and 300 K. In these conditions, dissociation was expected to be noticeable at the 10^{-4} s scale and the gas would be nearly in equilibrium under one second time. These are general expectations based on simulations using the macroscopic models of Park et al.[53] and Cruden et al.[16] We are not expecting to reproduce the aforementioned models but rather to obtain similar results within the limits of reasonability provided by the macroscopic models. Figure 10 presents in black the CO_2 mole fraction of this first simulation with the model

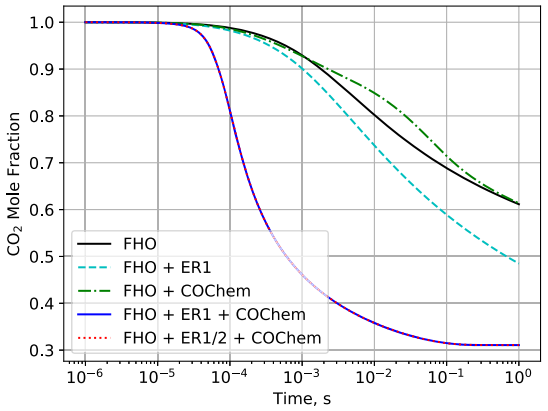

Figure 10. CO_2-simulated mole fraction in a 3690 m/s shock at 133 Pa in pure CO_2. The different lines correspond to the inclusion or exclusion of certain reactions. FHO corresponds to the model schematized in Figure 8. The inclusions of the exchange reaction $CO_2 + O \leftrightarrow CO + O_2$ (Sharipov), the $CO_2 + C \leftrightarrow CO + CO$, and the CO chemistry to the aforementioned FHO model are labeled ER1, ER2, and COChem, respectively. The reaction $CO_2 + O \leftrightarrow CO + O_2$ is seen to considerably enhance the dissociation of CO_2, reducing the characteristic decomposition time to 10^{-4}−10^{-5} s.

described so far. This result fails to meet the expected macroscopic physical behavior for these conditions as the flow has not equilibrated after 1 s. As such, other mechanisms important for CO_2 decomposition should be added to further complement the model. Usually, these chemical processes are not available in a state-to-state form. A reaction rate redistribution of a reaction rate may be carried out to transform a macroscopic reaction

$$CO_2 + X \leftrightarrow AB + CD \tag{12}$$

into a set of vibrational state-to-state rates of the same reaction

$$CO_2(X^1\Sigma, v) + X \leftrightarrow AB + CD \tag{13}$$

The redistribution employed in this work is identical to the one discussed in ref 54. A brief description is warranted here. Redistributing a macroscopic reaction rate to state-to-state reaction rates relies on the energy balance for a reaction. If the

https://dx.doi.org/10.1021/acs.jpca.0c05677
J. Phys. Chem. A XXXX, XXX, XXX−XXX

reagents have energy above the activation energy E_a, then the reaction is exothermic, otherwise the reaction is endothermic. E_a is taken as the balance of the enthalpies of formation between the products and reagents of the reaction or alternatively with the third Arrhenius coefficient θ converted to a suitable unit. We assume the shape of the exothermic state-to-state reactions to be

$$K_v(T) = A_v T^n \exp\left(-\frac{\theta}{T}\right) \tag{14}$$

and the endothermic state-to-state reactions to be

$$K_v(T) = B_v T^n \tag{15}$$

where A_v and B_v are the vibrational state-specific coefficients. We further assume that A_v has the shape

$$A_v = b\frac{E_a - E_v}{E_a - E_-} \tag{16}$$

and B_v has the shape

$$B_v = b\frac{E_+ - E_a}{E_v - E_a} \tag{17}$$

where b is some coefficient dependent on temperature, E_v is the energy of level v, E_- is the last level where the reaction is endothermic, and E_+ is the first level in which the reaction is exothermic. We then take a macroscopic reaction rate K_{macro} and enforce the equality to be true

$$K_{macro}(T) = \sum_v K_v(T)\frac{g_v \exp[-E_v/(k_B T)]}{Q_v} \tag{18}$$

where g_v is the degeneracy of level v, E_v is the energy of level v, and Q_v is the vibrational partition function of the considered levels for redistribution. Following the above equation, we substitute the assumed shapes for the state-to-state reaction rates and the functions of A_v and B_v to solve for b

$$b = \frac{K_{macro} Q_v}{\sum_{E=0}^{E_-}\frac{E_a - E_v}{E_a - E_-} g_v e^{-T_a/T} + \sum_{E_+}^{E_{max}}\frac{E_+ - E_a}{E_v - E_a} e^{-E_v/k_B T}} \tag{19}$$

This yields a state-to-state reaction rate set that is self-consistent with the initial macroscopic reaction rate. In this work, we only consider the vibrational manifold of the ground state of CO_2 for redistribution, assuming that the triplet CO_2 effects are negligible. This method should be considered a first approach to dealing with CO_2 vibrational excitation effects in exchange reactions. While the model described here assumes a 100% efficiency of vibrational excitation in lowering the activation energy, a more appropriate model would not assume so. The application of the α model, also known as the Macheret−Fridman model,[17,55−57] or the generalized Marrone−Treanor model (see, for example, ref 58) would be more appropriate. For now, this is left for a future revision of this work. Note that the pplication of said model would undoubtedly change the rate of decomposition for CO_2 (Figure 10). In conclusion the aforementioned figure shows the effect on CO_2 molar fraction for different stages of development of our FHO model, stages that will be explored in the next few subsections.

CO_2 + O ↔ CO + O_2 Exchange Processes. It has been experimentally observed that the addition of O atoms to the gas composition increases the dissociation rate of CO_2.[5252] This is usually attributed to the exchange reaction CO_2 + O ↔ CO + O_2. Table 5 presents some of the different exchange reaction rates found in the literature and considered for this work. Figure 11 plots the different reaction rate coefficients in the forward direction. It should be noted that several reactions are in qualitative agreement in the 1000−5000 K range, while two others are several orders of magnitude higher. Reactions 1 and 2 are taken from experimental studies[59,60] of the inverse reaction CO + O_2 → CO_2 + O. The first reported source is the original experiment, and the second is where the rate coefficient for the CO_2 + O → CO + O_2 reaction was reported. Reaction rate 3 from ref 61 is mentioned as an adaptation from ref 62 but it is not made clear how this adaptation was performed. Rate 4 was originally reported in ref 63. The original document could not be found and as such, it is not known whether this rate is experimental or calculated through other means. Rates 5−7 are presented as Arrhenius fit coefficients valid in the 800−5000 K range from QCT calculations carried out by Sharipov and Starik[64] on the CO + O_2 collision. Rate 5 assumes a Boltzmann distribution of the internal states for all intervening chemical species. Rates 6 and 7 are state-to-state rates corresponding to different seams of crossing between the CO + O_2 ground-state intermolecular potential and CO_2 + O intermolecular potential. The first crossing allows only the production of ground-state oxygen, $O(^3P)$, while the second crossing also produces $O(^1D)$.

Table 5. Reaction Rates for the CO_2 + O ↔ CO + O_2 (Direct or Inverse) Found in the Literature and Considered for This Work[a]

#	A (cm^3/(mol s))	n	θ (K)	notes	source
k_1	2.11×10^{13}	0.0	6651	2400−3000 K	59 , 62
k_2	2.10×10^{13}	0.0	27 800	1700−3500 K at 1.8 bar	53 , 60
k_3	2.14×10^{12}	0.0	22 848	adapted from k_1	61
k_4	2.71×10^{14}	0.0	33 800		16 , 63
k_5	4.32×10^{7}	1.618	25 018	inv. reac., 800−5000 K	64
k_6	7.63×10^{6}	1.670	26 950	$O(^3P)$, see k_5	64
k_7	5.18×10^{6}	1.728	33 470	$O(^1D)$ and $O(^3P)$, see k_5	64
k_8	2.88×10^{12}	0.0	24 005	inv. reac., set of exp.	65

[a]Reactions 1−4 are the rates for CO_2 + O → CO + O_2 and reactions 5−8 are for the inverse reaction.

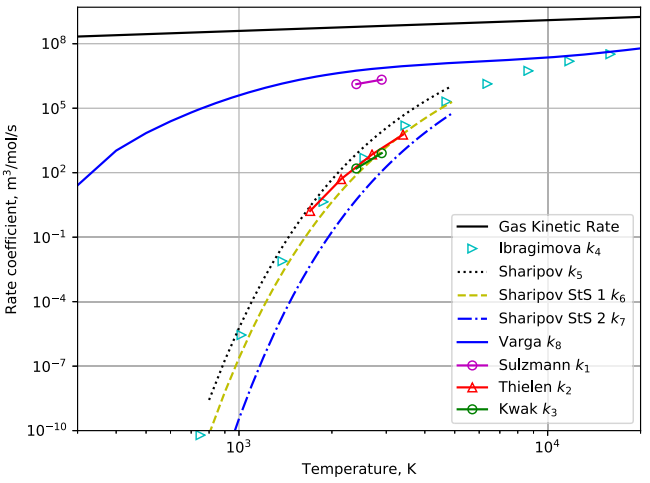

Figure 11. Exchange reactions CO_2 + O ↔ CO + O_2 found in some works in the literature plotted against the gas kinetic rate CO_2 + O collision.

https://dx.doi.org/10.1021/acs.jpca.0c05677
J. Phys. Chem. A XXXX, XXX, XXX−XXX

Table 6. Coefficients for the $CO + O_2 \rightarrow CO_2 + O$ Reactions 5−8 of Table 5 Using Equation 20[a]

	a	b	c	d	e	f	g	h	i
k_5	-4.071×10^{-1}	2.888×10^{0}	-3.693×10^{1}	-1.716×10^{0}	3.578×10^{1}	4.620×10^{-1}	-7.840×10^{-3}	6.734×10^{-5}	-2.220×10^{-7}
k_6	2.643×10^{-5}	2.072×10^{2}	-3.115×10^{1}	1.678×10^{0}	2.969×10^{1}	-5.880×10^{-4}	9.232×10^{-6}	-8.196×10^{-8}	2.877×10^{-10}
k_7	2.377×10^{-5}	2.073×10^{2}	-3.767×10^{1}	1.736×10^{0}	2.970×10^{1}	-5.871×10^{-4}	9.217×10^{-6}	-8.182×10^{-8}	2.872×10^{-10}
k_8	-4.071×10^{-1}	2.888×10^{0}	-1.194×10^{1}	-3.334×10^{0}	3.571×10^{1}	4.619×10^{-1}	-7.840×10^{-3}	6.734×10^{-5}	-2.219×10^{-7}

[a]Units are in $cm^3/(mol\ s)$.

The authors of ref 64 decided not to branch the production of different O levels as this reaction is negligible compared to others presented in the same work. An additional reaction is presented in ref 64 where $CO + O_2(a)$ produces $CO_2 + O$ however the contribution of $O_2(a)$ will be neglected in this work and considered only for future developments of this model. Finally, rate 8 coefficients were obtained from sensitivity analysis of combustion experiments in Varga Ph.D. thesis[65] and reported to have low uncertainty. An inversion of rates 5−8 was performed using the SPARK code by computing the partition functions of intervening molecules and the equilibrium constant of the $CO + O_2 \leftrightarrow CO_2 + O$ reaction. As such, the presented 5−8 rates in Table 5 correspond to the $CO + O_2 \rightarrow CO_2 + O$ inverse reaction. The forward reaction rates were fitted through a ninth-order polynomial such as

$$K = \exp\left(\frac{a}{\overline{T}^3} + \frac{b}{\overline{T}^2} + \frac{c}{\overline{T}} + d\log(\overline{T}) + e + f\overline{T} + g\overline{T}^2 + h\overline{T}^3 + i\overline{T}^4\right) \tag{20}$$

The coefficients for reactions 5−8 using the above equation are reported in Table 6. Reaction rates 1−5 and 8 were assumed to involve only the ground state of each chemical species. Reactions 6 and 7 were used to derive a reaction rate coefficient for the $CO_2 + O(^3P) \leftrightarrow CO + O_2$ and $CO_2 + O(^1D) \leftrightarrow CO + O_2$ reactions by assuming a 50:50 branching for O atoms in rate 7. The addition of k_6 and half of k_7 are labeled as "Sharipov StS 1" and half of k_7 is labeled as "Sharipov StS 2" in Figure 11 where these rate coefficients are plotted along with k_1 to k_5 and k_8 of Table 5. The gas kinetic rate coefficient for the $CO_2 + O$ collision is also plotted in black in the same figure. Back to Figure 10, the curve with the redistributed $CO_2 + O$ exchange reaction reported by Sharipov[64] and denoted k_5 in Table 5 is plotted with the label "FHO + ER". An improvement to the previous model is obtained but still far from an equilibrium state at the second time scale.

The preliminary results already show that the $CO_2 + O$ collision is of importance to CO_2 processes. This work will limit itself to including CO_2 vibrational excitation effects in this reaction. However, the vibronic (vibrational + electronic) excitation of CO_2, O_2, and CO as well as the electronic excitation of O atoms should not be underestimated. The work of Kustova et al.,[58] for instance, explores the question of the role of vibrational excited CO_2, O_2, and CO molecules in the overall dissociation and recombination of CO_2. At low temperatures and for low vibrational numbers, the analysis reveals a CO_2 dissociation driven by the exchange reaction rather than the $CO_2 + M \leftrightarrow CO + O + M$. In an radio frequency (RF) CO_2 plasma, experimentally assessed by Morillo-Candas et al.,[66] the electronically excited CO(a) favorably reacts with O_2 to yield $CO_2 + O$. Additionally, as suggested by the aforementioned third StS reaction of Sharipov,[64] the excited-state $O_2(a)$ might also be important for the back-reaction. Improvements in this area and inclusion of excited states for other species might considerably affect the results contained in this work.

$CO_2 + C \leftrightarrow CO + CO$ Exchange Reaction. An important reaction in industrial processes is the Boudouard reaction $2\ CO \leftrightarrow CO_2 + C$. In the aforementioned processes, this usually involves a phase change of the product carbon and is one of the reactions responsible for the creation of soot. Therefore, most available data do not consider all chemical species in the gaseous phase. The NIST Chemical Kinetics Database contains two estimates for the reaction rate coefficient at 300 K for the reaction $CO_2 + C \rightarrow 2\ CO$. We will take the lowest estimate, which is also the most recent[67] as $k_f = 6.022 \times 10^8\ cm^3/(mol\ s)$. We give a temperature dependence to this reaction as

$$k_f(T) = \frac{k_f(300\ K)}{Z(300\ K)}Z(T) \tag{21}$$

where $Z(T)$ is the $CO_2 + C$ gas kinetic rate coefficient. This formulation may be interpreted as the total ratio of collisions $CO_2 + C$ to collisions resulting in CO + CO or other products is constant. After the expansion, a redistribution as described in this section is carried out. Despite being an important industrial process, in the gaseous phase, this reaction is not expected to be important since C atoms are very reactive and fastly disappear in gaseous environments to form other compounds. It is included just for the sake of completeness. Therefore the reaction is represented in Figure 10 with the label "FHO + ER1/2 + COChem". As a relatively negligible process, it did not justify a simulation by itself, and was added to the previously discussed mechanisms.

Quenching of O Atoms. Quenching of atomic O is also introduced in the model. Specifically, the reaction $O(^1D) + M \leftrightarrow O(^3P) + M$ is addressed with data from the literature. Before that, a brief discussion on the importance of this mechanism is carried out here. The appendix of the work of Fox and Hać[68] provides an extensive review of cooling mechanisms for hot O atoms. These hot atoms need not be electronically excited O: even translationally excited $O(^3P)$ atoms may redistribute their energy to the rovibrational modes of molecules. Important collision partners are CO, O_2, and CO_2. One contribution[69] has even reported an efficient deposition of translational energy into the rovibrational modes of CO_2. Additionally, the importance of the excited $O(^1D)$ atom cannot be understated as its excess energy may be redistributed to vibrationally excited O_2 and CO_2 molecules through the reactions: $O(^1D) + CO_2 \leftrightarrow O_2(v, J) + CO + 1.63$ eV and $O(^1D) + CO_2 \leftrightarrow O(^3P) + CO_2(v, J) + 1.97$ eV. However, in this work, we will only deal with quenching reactions like $O(^1D) + M \leftrightarrow O(^3P) + M$. Some measurements of the reaction rate coefficients at 300 K are summarized in Table 7. These reactions are given a temperature dependence according to eq 21 and fitted to an Arrhenius rates

$$k_f = AT^n \exp\left(-\frac{\theta}{T}\right) \tag{22}$$

https://dx.doi.org/10.1021/acs.jpca.0c05677
J. Phys. Chem. A XXXX, XXX, XXX−XXX

Table 7. Quenching Reaction Rates of $O(^1D) + M \leftrightarrow O(^3P) + M$ at 300 K[a]

M	CO_2	CO	O_2
k_f	1.03	0.3	0.41
source	71	72	73

[a]Units are 10^{-10} $cm^3/(part\ s)$.

A reaction rate coefficient with partner $O(^3P)$ is also available from ref 70 but with no temperature validity range, and with the shape

$$k_f = A + B\sqrt{T} + CT \tag{23}$$

and coefficients $A = 7.66 \times 10^{-12}$, $B = 2.13 \times 10^{-13}$, and $C = -1.84 \times 10^{-15}$ in units of $cm^3/(part\ s)$. An Arrhenius fit was performed on this reaction from 300 up to 2500 K and checked for consistency up to 100 000 K. The Arrhenius coefficients of the fitted O quenching reactions are found in Table 8.

Table 8. Quenching Reaction Rates of $O(^1D) + M \leftrightarrow O(^3P) + M$ Fitted to Arrhenius Expressions

M	CO_2	CO	O_2	$O(^1D)$
A ($10^{12} cm^3/(mol\ s)$)	3.58	1.04	1.43	4.21
n	0.50	0.50	0.50	0.088
θ (K)	0.00	0.00	0.00	21.91

Other Rates. Other processes, not directly related to CO_2, could still make an impact on the concentration of CO_2. As such, we have included the thermochemistry for CO, reported in the work of Cruden et al.,[16] into our kinetic model. In these reactions, we have assumed that O is in its ground state. The rates we have included are presented in Table 9. In Figure 10, the label "COChem" indicates the inclusion of the reactions in Table 9 of the simulation. In the curve with label "FHO + COChem", the CO_2 mole fraction is closer to the base "FHO" model than the curves with the exchange reaction $CO_2 + O \leftrightarrow CO + O_2$ labeled "FHO + ER1", "FHO + ER1 + COChem", and "FHO + ER1/2 + COChem". The latter curves indicate that the inclusion of the $CO_2 + O$ exchange reaction is essential to obtain a better dissociation trend for CO_2. Adding the thermochemistry in ref 16 provides a source of O atoms, which accelerate CO_2 decomposition.

Final Data Set. To summarize the model developed in this work, reaction labels and the number of reactions are presented in Table 10. This excludes the macroscopic reactions from ref 16 since these are presented in Table 9. There are 11 species in the model: CO_2, CO, O_2, C_2, C, O, CO^+, O_2^+, C^+, O^+, and e^-, 2 of which are state-specific, CO_2 with 201 vibronic levels and O with 2 electronic levels. The model contains a total of 22 569 reactions, only 14 of which are not state-specific.

Underlying Assumptions and Restrictions. CO_2 is a triatomic molecule, and consequently, has more degrees of freedom than a diatomic molecule. This induces complexities in the sense that modeling for such molecules needs to be tractable with a reasonable number of levels and rates, compatible with present-day computational resources. In this sense, much more restrictions and assumptions than in the case of diatomic molecules need to be brought. For example, diatomic molecule state-to-state models customarily assume a Boltzmann equilibrium for the rotational levels, solely modeling a reasonable number of vibrational and electronic states (in order of the hundred). For CO_2, not only this has to be assumed, but furthermore, additional restrictions have to be brought regarding the different vibrational degrees of freedom. These include:

- Full separation of the three vibrational modes of CO_2, only considering its so-called extreme states. An extreme state is a state which is only part of a single mode, in our model it implies that no mixed-mode states are treated. Calculations by Billing[80] show that differences from a factor of 5 (at room temperature) down to a factor of 1.5 (at 2000 K) exist for rate coefficients between the same v_1 and v_3 but with different v_2. This is perhaps the most significant limitation of our model, with implications on the modeling of higher, near-dissociation levels, which we will discuss more ahead. Nevertheless, this allows us to achieve a computationally tractable model with about $N \approx 250$ levels instead of the $N \approx 10\,000^+$ real ground-state levels of CO_2.
- For the same reasons, there is no specific accounting of the l_2 bending quantum numbers. Billing calculations from ref 81 predict differences ranging from a factor of 5 to 10 in transitions from the same v_2 level, depending on the l_2 quantum number.
- We extrapolate the CO_2 PES in its three mode limits (*ss*, *be*, *as*) by a representative repulsive and near-dissociation

Table 9. Reactions and Corresponding Arrhenius Coefficients Proposed in Ref 16

reaction	A ($cm^3/(mol\ s)$)	n	θ (K)	source
$CO + M \leftrightarrow C + O + M$	7.99×10^{38}	−5.5	129 000	74
$C_2 + O \leftrightarrow CO + C$	3.61×10^{14}	0.0	0.0	75
$C_2 + M \leftrightarrow C + C + M$	1.82×10^{15}	0.0	64 000	75
$CO + O \leftrightarrow C + O_2$	3.9×10^{13}	−0.18	69 200	53
$O_2 + M \leftrightarrow O + O + M$	1.2×10^{14}	0.0	54 246	76
$C + e^- \leftrightarrow C^+ + e^- + e^-$	3.7×10^{31}	−3.0	130 700	53
$O + e^- \leftrightarrow O^+ + e^- + e^-$	3.9×10^{33}	−3.78	158 500	77
$CO + e^- \leftrightarrow CO^+ + e^- + e^-$	4.5×10^{14}	0.275	163 500	78
$O_2 + e^- \leftrightarrow O_2^+ + e^- + e^-$	2.19×10^{10}	1.16	130 000	78
$C + O \leftrightarrow CO^+ + e^-$	8.8×10^{8}	1.0	33 100	53
$CO + C^+ \leftrightarrow CO^+ + C$	1.1×10^{13}	0.0	31 400	53
$O + O \leftrightarrow O_2^+ + e^-$	7.1×10^{2}	2.7	80 600	79
$O_2 + C^+ \leftrightarrow O_2^+ + C$	1.0×10^{13}	0.0	9400	53
$O_2^+ + O \leftrightarrow O_2 + O^+$	2.19×10^{10}	1.16	130 000	79

https://dx.doi.org/10.1021/acs.jpca.0c05677
J. Phys. Chem. A XXXX, XXX, XXX−XXX

Table 10. List of Reactions Included in Our CO_2 Kinetic Model[a]

	name	type	#reac.
R1	$CO_2(X,v_1') + M \leftrightarrow CO_2(X,v_1'') + M$	VT	1770
R2	$CO_2(X,v_2') + M \leftrightarrow CO_2(X,v_2'') + M$	VT	5050
R3	$CO_2(X,v_3') + M \leftrightarrow CO_2(X,v_3'') + M$	VT	861
R4	$CO_2(X,v_1') + CO_2(X,v'_1) \leftrightarrow CO_2(X,v_1'+1) + CO_2(X,v_1' - 1)$	VVT	58
R5	$CO_2(X,v_2') + CO_2(X,v'_2) \leftrightarrow CO_2(X,v_2'+1) + CO_2(X,v_2' - 1)$	VVT	99
R6	$CO_2(X,v_3') + CO_2(X,v'_3) \leftrightarrow CO_2(X,v_3'+1) + CO_2(X,v_3' - 1)$	VVT	41
R7	$CO_2(X,v_1') + M \leftrightarrow CO_2(X,v_2'') + M$	IVT	5900
R8	$CO_2(X,v_1') + M \leftrightarrow CO_2(X,v_3'') + M$	IVT	2478
R9	$CO_2(X,v_2') + M \leftrightarrow CO_2(X,v_3'') + M$	IVT	4200
R10	$CO_2(B,v_1') + M \leftrightarrow CO_2(B,v_1'') + M$	VT	78
R11	$CO_2(B,v_2') + M \leftrightarrow CO_2(B,v_2'') + M$	VT	325
R12	$CO_2(B,v_3') + M \leftrightarrow CO_2(B,v_3'') + M$	VT	21
R13	$CO_2(B,v_1') + CO_2(B,v'_1) \leftrightarrow CO_2(B,v_1'+1) + CO_2(B,v_1' - 1)$	VVT	11
R14	$CO_2(B,v_2') + CO_2(B,v'_2) \leftrightarrow CO_2(B,v_2'+1) + CO_2(B,v_2' - 1)$	VVT	24
R15	$CO_2(B,v_3') + CO_2(B,v'_3) \leftrightarrow CO_2(B,v_3'+1) + CO_2(B,v_3' - 1)$	VVT	6
R16	$CO_2(B,v_1') + M \leftrightarrow CO_2(B,v_2'') + M$	IVT	300
R17	$CO_2(B,v_1') + M \leftrightarrow CO_2(B,v_3'') + M$	IVT	84
R18	$CO_2(B,v_2') + M \leftrightarrow CO_2(B,v_3'') + M$	IVT	175
R19	$CO_2(X,v_2') + M \leftrightarrow CO_2(B,v_1'') + M$	VE	103
R20	$CO_2(X,v_2') + M \leftrightarrow CO_2(B,v_2'') + M$	VE	311
R21	$CO_2(X,v_2') + M \leftrightarrow CO_2(B,v_3'') + M$	VE	163
R22	$CO_2(X,v_3') + M \leftrightarrow CO + O(^1D) + M$	VD	42
R23	$CO_2(X,v_3') + M \leftrightarrow CO + O(^3P) + M$	VE/VD	42
R24	$CO_2(B,v_3') + M \leftrightarrow CO + O(^3P) + M$	VD	7
R25	$CO_2(X,v'_{1,2,3}) + O(^3P) \leftrightarrow CO + O_2$	exchange	201
R26	$CO_2(X,v'_{1,2,3}) + C \leftrightarrow CO + CO$	exchange	201
R27	$O(^1D) + M \leftrightarrow O(^3P) + M$	quench.	4

[a]Not listed are the reactions taken from the kinetic scheme in ref 16, which describes CO thermochemistry. These reactions can be found in Table 9.

potential. While this is not as accurate as defining a proper PES near-dissociation potential (which is not carried out in the NASA-Ames-2 PES), we should still be capable of providing correct near-dissociation trends, as compared with the usual extrapolation of polynomial expansions. Past similar approaches for diatomic molecules have provided quite accurate results.[24]

In addition to those, other limitations currently exist but could easily be waived in future works:

- Considering an isotropic Morse-like intermolecular potential, and assuming the collision as 1D with the application of a steric factor. Comparisons carried out with the FHO model against PES-based methods show that rates with the same order of magnitude are predicted. However, the temperature dependence at low temperatures is poorly reproduced by the FHO model, and attractive low-temperature effects should be modeled resorting to the Sharma−Brau[82] theory and added to the rate provided by the FHO theory. Results in the higher-temperature limit have a better agreement with PES results, as would be expected in the Landau−Teller limit (increasing $\log(K_f)$ over $T^{-1/3}$). Regarding the scaling of rates to higher-vibrational quantum levels, there is not enough PES-based data to provide a meaningful comparison. Nevertheless, since this work is mostly concerned with mid-to-high-temperature regimes, we may safely neglect these low-temperature limits below room temperature.
- The rates of collision are the same independently of the collisional partner, which is assumed to be CO_2. This assumption is temporarily used as a matter of convenience since our worked examples are applied to pure CO_2 flows. This assumption will need to be revisited for increasing the accuracy of the database or allowing for simulations of highly diluted CO_2 flows (typically in helium or argon baths).

RESULTS

The results of the developed model are shown and discussed in this section. First, we present and discuss some of the calculated rates in Table 10. Then, we showcase simulations for an isothermal excitation of a gas with no dissociation, a post-shock relaxation of a gas, including dissociation and recombination reactions, a recombination to 1000 K from an equilibrium gas at 5000 K, and we conclude with a comparison against available shock-tube experiments.

Rate Data Set. This subsection will present some of the calculated rates presented in Table 10, notably, mechanisms R2, R7, and R23. Mechanisms R1−R3 to R10−R12 share the same functional form. The same can be said for mechanisms R7−R9 and R16−R18. Reactions that involve a spin-forbidden interaction such as R19, R20, R21, and R23 also share some similarities.

Firstly, in Figure 12, the $\log_{10}(K_{VT})$ rate coefficients of the bending levels of the ground electronic state of CO_2 are shown at 5000 K. These correspond to the rate coefficients of mechanism R2 in Table 10. It is expected that transitions with small differences in the vibrational number should be stronger than those with greater Δv. This is observed as the rate coefficients tend to a maximum value around the plane where $v_2' = v_2''$. The

https://dx.doi.org/10.1021/acs.jpca.0c05677
J. Phys. Chem. A XXXX, XXX, XXX−XXX

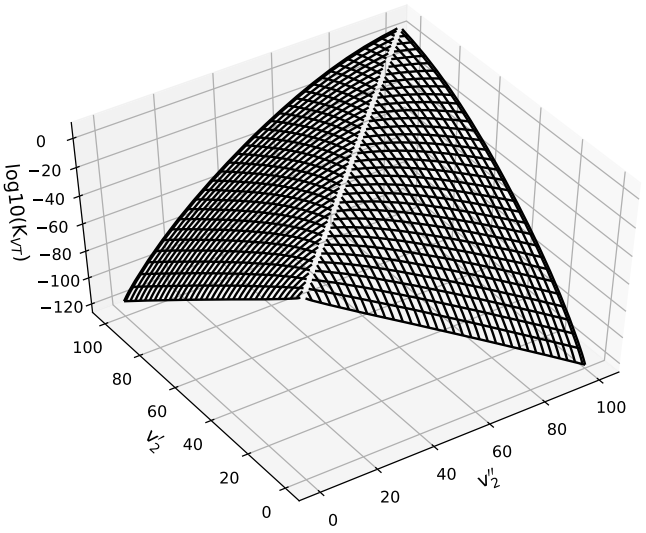

Figure 12. Base 10 logarithm of VT rate coefficients at 5000 K for the bending mode of CO_2. As expected, large quantum jumps have lower probability than smaller jumps, with endothermic jumps falling out faster than the reverse exothermic jumps. VT rate coefficients of other modes have the same functional shape.

reactions with no change in vibrational number are not depicted as these correspond to no energy exchange happening. Two oblique surfaces corresponding to exothermic and endothermic reactions are observed. The exothermic reactions are slightly more likely than endothermic reactions, and this is also observed by comparing the inclination of the surfaces against the z axis scale in the planes $v_2' = 100$ and $v_2'' = 100$. Reaction mechanisms R1−R3 and R10−R12 are functionally the same as R2 with some deformations that might occur when the Bessel approximation[33] is used.

Secondly, in Figure 13, the $\log_{10}(K_{IVT})$ rate coefficients between the bending and symmetric stretch levels of ground CO_2 are shown at 5000 K. These processes correspond to mechanism R7 in Table 10. As these transition probabilities are modeled as the product of two VT transitions with large changes

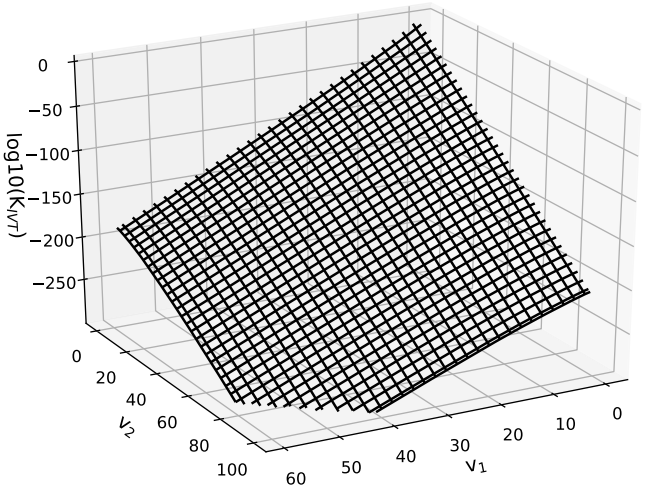

Figure 13. Base 10 logarithm of IVT rate coefficients at 5000 K between the symmetric and bending modes of CO_2. As expected, the probability of intermode energy exchange is lowest when the vibrational numbers are high and highest when the vibrational numbers are low. Other IVT rate coefficient sets have the same functional shape.

in vibrational number, the rate coefficients drop very fast as the vibrational numbers increase. Reaction mechanisms R8, R9, and R16−R18 share the same functional form as mechanism R7.

Finally, in Figure 14, the rate coefficients of mechanism R23 in Table 10 are plotted at 1000, 2000, and 3000 K. A maximum for

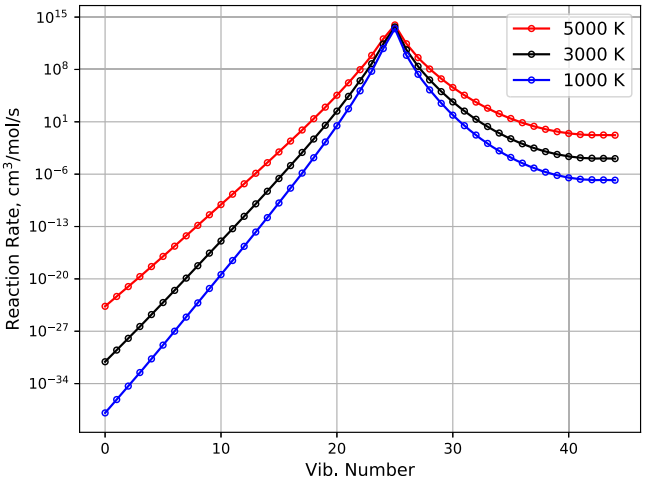

Figure 14. Rate coefficients computed using the Rosen−Zener probability formula (eq 11) for the dissociation mechanism R23 in Table 10. The rate coefficients are computed at 1000, 3000, and 5000 K, and as expected, the greater transition probabilities lie close to the crossing point between the singlet and triplet CO_2. Exothermic reactions (right of the maximum) are more probable than endothermic reactions (left of the maximum).

the rate coefficient is observed at the vibrational number, which is closest to the crossing between the ground state of CO_2 and the repulsive triplet state of CO_2. This is expected according to the simple formulation of the Rosen−Zener probability formula in eq 11. Mechanisms R19, R20, and R21 are also computed through the same formula and may have different crossings, which will correspond to horizontal shifts in the peak of the rate coefficients plotted in Figure 14. Otherwise, the aforementioned mechanisms share the same functional form as R23.

Theoretical Test Cases. *CO_2 Isothermal.* An isothermal 0D simulation was performed for a pure CO_2 gas, initially at 300 K and 2000 Pa with the gas temperature suddenly increased to 5000 K. For this particular simulation, we have decided to disregard dissociation processes and consider only excitation processes for CO_2. Time snapshots of the mass fractions of CO_2 are plotted in Figure 15. In the top-left figure, at $t = 8.52 \times 10^{-7}$ s, the bending mode is excited much faster than the other modes. This is expected since the spacing between consecutive vibrational levels is smaller. The electronically excited CO_2 accompanies the excitation of the bending mode, which gets more populated than the levels at the same energy of the asymmetric and symmetric stretch modes of the ground state of CO_2. Contrary to expectations, the asymmetric mode is more populated than the symmetric stretch mode. That changes at $t = 2.92 \times 10^{-5}$ s in the top right of Figure 15. At this time, the symmetric stretch mode overtakes the asymmetric stretch mode of the CO_2 ground state, except in the higher energy levels of the asymmetric stretch mode. At $t = 3.18 \times 10^{-4}$ s, the bending mode and the CO_2 triplet state are almost in their equilibrium populations. At $t = 1.14 \times 10^{-2}$ s, all CO_2 subpopulations are in equilibrium except the asymmetric stretch mode. From these simulations and considering the possible pathways for CO_2

https://dx.doi.org/10.1021/acs.jpca.0c05677
J. Phys. Chem. A XXXX, XXX, XXX−XXX

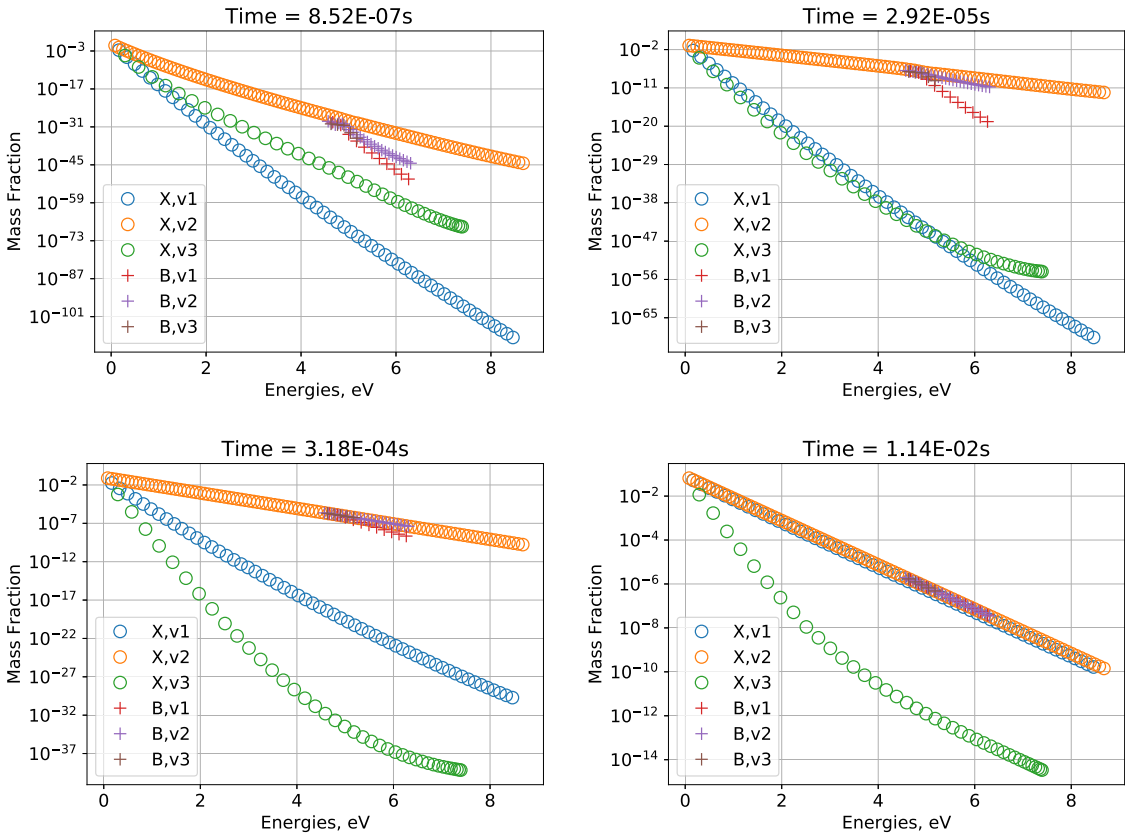

Figure 15. Time snapshots of the CO_2 vibrational distribution in a 0D isothermal simulation for a pure CO_2 gas at 2000 Pa initially at 300 K and a final temperature of 5000 K.

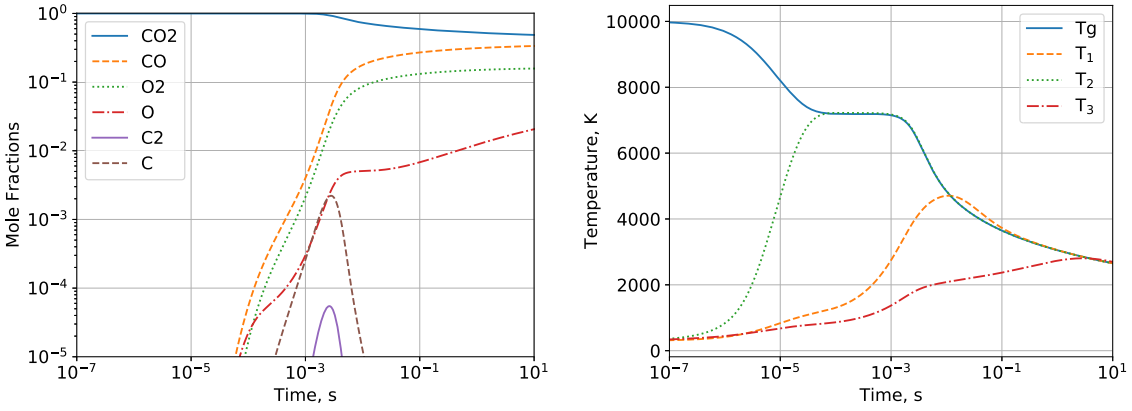

Figure 16. Mole fractions (left) and temperatures (right) of a CO_2 gas initially at 300 K and 2000 Pa suddenly heated to 10 000 K in a 0D simulation.

dissociation, it is expectable that the greatest contributor to CO_2 dissociation is the pathway through the excited triplet state of CO_2 (mechanism R24).

CO_2 Dissociating Flow. Another 0D simulation was performed again in a pure CO_2 gas initially at 300 K and 2000 Pa, which is suddenly heated to 10 000 K and allowed to relax and dissociate. The mole fractions are plotted on the left in Figure 16. On the right, the gas temperature, and the characteristic equivalent vibrational temperatures that yield Boltzmann distributions with the same energy than the non-Boltzmann distributions for each vibrational mode, are presented. There are several features that should already be expected from the discussion of the previous test case. Firstly, the relative distribution of vibrational modes of CO_2 is in agreement with the distributions in Figure 15, except now the gas is not isothermal and as such the temperature continuously drops until thermal equilibrium is achieved. Secondly, as seen in Figure 10, the exchange reaction $CO_2 + O \leftrightarrow CO + O_2$ dominates the decomposition of CO_2 as the creation of CO and O_2 far outpaces the production of O atoms, which are created mostly through the VD reactions calculated through the FHO or Rosen−Zener dissociation models. Additionally, the initial temperature decay from 10^{-7} to 10^{-5} s stems mostly from the excitation of the bending mode and the exchange reaction $CO_2 + O \leftrightarrow CO + O_2$, which is very efficient energy-wise as the gas temperature is mostly constant between 10^{-4} and 10^{-3} when the aforementioned reaction is most active. Beyond 10^{-3} s, chemistry becomes the most active process with dissociation of C_2 molecules into C atoms. Around 10^{-2} s, CO_2 vibrational modes are in equilibrium with each other.

https://dx.doi.org/10.1021/acs.jpca.0c05677
J. Phys. Chem. A XXXX, XXX, XXX−XXX

CO_2 Recombining Flow. A third and final 0D simulation attempts to capture the recombination dynamics of CO_2. The equilibrium composition of a CO_2, CO, O_2, C_2, C, and O gas and their respective ions and electrons was determined at 5000 K using the SPARK code. A very similar mixture, to round the sum of all molar fractions to 1, is determined and left at 1000 K and 1 bar with the isothermal conditions enforced. This simulation is performed twice with the $CO_2 + O \leftrightarrow CO + O_2$ rate by Sharipov[64] or Varga,[65] respectively. These reactions are over 9 orders of magnitude different at 1000 K as can be seen in Figure 11. It is also worth mentioning that, although most rate coefficients in Figure 11 agree with the rate from Sharipov, the rate from Varga is obtained from a sensitivity analysis of experimental data of combustion experiments. As such, it is not a whimsical comparison but a demonstration of the disparity of the $CO_2 + O$ reaction rate estimate at low temperatures. The mole fractions of this simulation are plotted in Figure 17 with the simple lines using the Sharipov rate and the lines with circles using the Varga rate. Very quickly, C atoms and C_2 molecules disappear from the gas and as such are not displayed in the figure. C^+ atoms recombine slower, O^+ and e^- take somewhat longer to recombine, and their temporal variation is very similar. For the simulation using Sharipov's rate, O atoms start recombining into O_2 molecules at around 10^{-8} s and further combine with CO to form CO_2 at 10^4 s. At around 10^1, CO_2 starts to recombine and is fully recombined around 10^6 s. In contrast, the simulation using Varga's rate shows similar times for the recombination of O_2 and CO_2. The O_2 molecule concentrations diverge from the Sharipov simulation after 10^{-7} s to react with CO to create more CO_2. The O atoms are consumed more rapidly than CO and O_2 molecules. O atoms may recombine into O_2, or into CO_2 if CO is present in enough concentrations. CO and O_2 molecules recombine into CO_2, with the additional formation of O atoms. CO_2 becomes fully recombined by 10^{-2} s. It is clear that the exchange reaction $CO_2 + O \leftrightarrow CO + O_2$ is an essential mechanism in the recombination of CO_2. Its importance and the need to obtain accurate estimates of the reaction rate of this process at low temperatures should not be understated. A recent experimental study[83] indicates the typical recombination times of CO_2 in the postdischarge of a microwave plasma at not too different conditions on the order of the millisecond. This result is more in line with the simulations performed using the Varga rate, which indicates better suitability of this reaction rate.

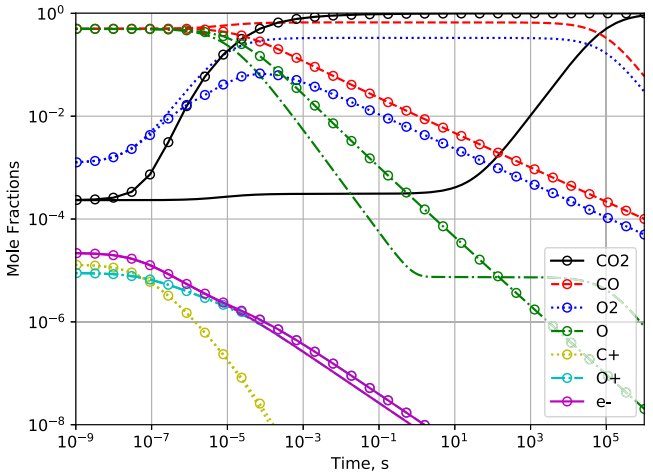

Figure 17. Mole fractions for the C and O compounds and ions in a recombining isothermal gas kept at 1000 K and 1 bar in a 0D simulation. The lines with circles correspond to the simulations using Varga $CO_2 + O \leftrightarrow CO + O_2$ rate and those without circles to the simulations using Sharipov's rate.

Comparison with Shock-Tube Experiments. In 2008, a shock-tube campaign was carried out in the Moscow Institute of Physics and Technology (MIPT) under a contract from the European Space Agency (ESA).[36,84−90] The objective of the study was to validate the existing CFD tools employed in the design of the EXOMARS mission. Among the deployed diagnostics, a mercury lamp was used to measure the absorbance of the flow in the hot $CO_2(B \rightarrow X)$ UV band around 253.7 nm. This allows measuring the time evolution of the concentration in the ground state and an estimation of the decomposition time behind the shock. Seven shots were performed using this diagnostic as per Table 11 with initial temperatures of $T = 300$ K and the test gas fully composed of CO_2. One-dimensional simulations, using the CO_2 FHO model described in this work, were carried out using the conditions of Table 11 as the upstream conditions. Different simulations were carried out, using different reaction rate coefficients for the $CO_2 + O \leftrightarrow CO + O_2$ exchange reaction. For simulated species concentration profiles, defining a characteristic decomposition time is more difficult than for an experimental signal. In a simulated profile, it is not as straightforward to define the incubation time as it is for an experimental signal. In this work, we have defined the following criterion for computing the decomposition time: the instant at which the derivative of the molar fraction of CO_2 is at its lowest. In other words, the decomposition time is when the molar fraction changes curvature, which represents the moment where the flow is in a quasi-steady-state. In contrast, an example of the experimental measurements performed at MIPT is shown in Figure 18 with an estimation of the decomposition time. There is a rise in the absorption signal of CO_2 at 30 μs, which corresponds to the increase of density after the passage of the shock wave. At 60 μs, the arrival of the contact wave marks the end of the useful flow.

The simulation results are presented in Figure 19 with experimental points reported against the results of the FHO model with the exchange reactions described in the Macroscopic Chemistry section and the rate from Varga[65] considering the typical interval of F.C. factors. The lowest velocity point, near 3000 m/s, is overestimated by all exchange rate coefficients except by Thielen. In fact, the simulations with this shock velocity do not have any physical significance as the model does not capture any significant dissociation. Therefore, we will ignore this point for the remainder of this analysis. As the shock

Table 11. Shock Characteristics of the Experimental Campaign Carried out in MIPT

shot #	1	2	3	4	5	6	7
pressure (Torr)	8.8	9.0	6.5	8.0	5.9	6.2	5.6
velocity (m/s)	3020	3340	3370	3370	3450	3470	3620
incubation time (μs)	35	17	12	14	9	13	2

https://dx.doi.org/10.1021/acs.jpca.0c05677
J. Phys. Chem. A XXXX, XXX, XXX−XXX

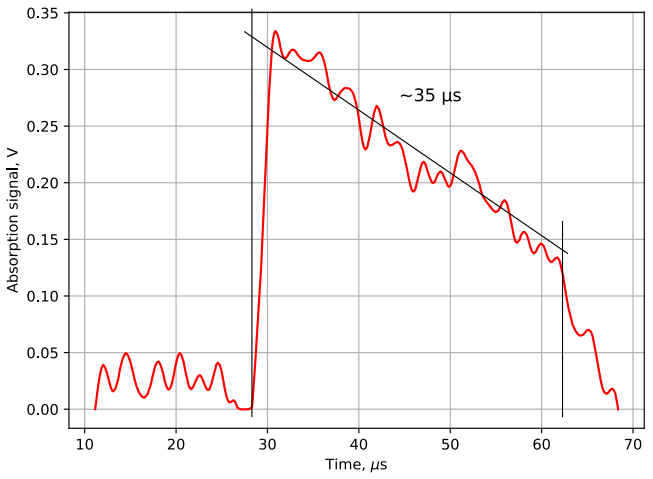

Figure 18. Experimental measurement of CO_2 absorbance in a shock tube. The shock velocity was 3020 m/s, and the pressure in the tube was 8.8 Torr corresponding to the first shot in Table 11 and the left-most point in Figure 19. Here, the useful test time lies between 30 μs with the arrival of the shock wave and 60 μs with the arrival of the contact wave. The black lines show how the time of decomposition may be estimated in these measurements.

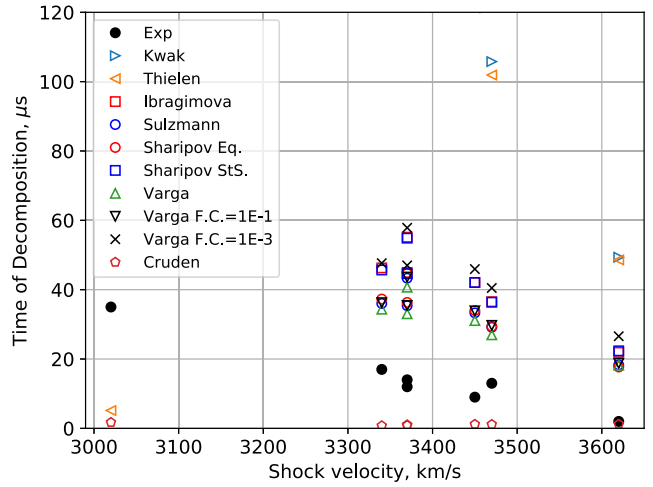

Figure 19. Time of decomposition for several shocks in pure CO_2. Experimental points are plotted in full circles and calculated points with other symbols. A linear relationship between increasing shock speed and decreasing decomposition time is observed in experimental and calculated points.

velocity increases, the time of decomposition decreases in a linear fashion independently of pressure. This trend is observed with whatever exchange reaction is used with the model, the slope of the trend being what changes with the considered exchange reaction. The best results are achieved with the redistributed state-to-state reactions from Varga,[65] and good estimates are also achieved with the rates from Sulzmann, Ibragimova, and Sharipov.[59,63,64] Considering the F.C. factors and the exchange rate proposed by Varga, the decomposition time increase in the range 2.3−16.6 μs if the higher and lower limits for the typical F.C. factors are used, respectively. The results obtained from Thielen and Kwak[60,61] do not provide a good estimate but also showcase a linear trend. Also plotted with these models is the macroscopic model presented by Cruden et al. in ref 16. This macroscopic model underestimates the time of decomposition and does not yield the same linear trend that is expected from the experiments and other models. This may be due more to the underlying assumption of a Boltzmann distribution for the internal states, rather than any inherent inadequacy of the proposed macroscopic kinetic rates.

DISCUSSION

We have presented a vibrational state-to-state kinetic model for CO_2 with a number of improvements over current state-of-the-art models. First, the forced harmonic oscillator theory has been for the first time extended to linear triatomic molecules such as CO_2 and deployed in a complete and self-contained state-to-state kinetic model tailored for heavy-impact reactions. This is a significant improvement compared to the traditional SSH scaling laws commonly used. Instead of carrying a scaling of experimental rates, we estimate the different intermolecular potentials that reproduce such experimentally determined rates and then use these same parameters to calculate the FHO rates over the whole vibrational energies manifold. Furthermore, by using the general FHO theory instead of first-order perturbation theories such as the SSH model, we avoid obtaining transition probabilities above one in the high-temperature regime and in the near-dissociation limit, where energy spacings become ever smaller. These are well-known shortcomings of the SSH theory.[15] More importantly, we may now account for multi-quantum transitions, which are well known to become important in higher-temperature regimes.[15]

A second improvement against the current status-quo is provided by the detailed discussion on the crossings between the ground and electronic states of CO_2, which is treated in a much more consistent fashion than in past works, which make the more naïve assumption of an asymmetric mode crossing from the linear ground-state configuration of CO_2 to a near-dissociative vibrational level for the 70° bent excited-state configuration around 5.52 eV. Instead, from the analysis of published PES, we find that PES crossings may instead arise from the bent v_2 mode crossing at 4.99 eV or through the asymmetric stretch mode v_3 crossing at 5.85 eV. In this last case, the excited state is repulsive and the CO_2 molecule is allowed to dissociate immediately after the crossing.

Ultimately, these two improvements are overshadowed by the findings that the $CO_2 + O \leftrightarrow CO + O_2$ reaction is quintessential to both the dissociation and recombination dynamics of CO_2. Indeed, it has been found that without the inclusion of this rate, direct dissociation and recombination processes of CO_2 become unrealistically slow, hinting that dissociation for CO_2 is likely to follow a two-step process where direct dissociation of CO_2 creates a first batch of atomic oxygen atoms O, which then induce further decomposition of CO_2 into CO and O_2 products.

Future Improvements. There are several potential pathways for improvement of the presented model, which will be discussed here briefly in no particular order. Firstly, collisional partners other than CO_2 should be included in the model. This would require a straightforward review and calibration of the FHO model against further experimental rates, in the exact same fashion that was carried out in the development of this model. However, this will at most lead to a 5-fold increase in the number of rates in the model. The quality-of-life improvements in the model will have to be weighed against the computational overhead. Secondly, the state-to-state kinetics for diatomic molecules could be added for a further sophistication of the model. These rates have been reasonably well modeled in the past.[13,36] Thirdly, a better treatment of the exchange reaction $CO_2 + O \leftrightarrow CO + O_2$ should be considered and possibly the

https://dx.doi.org/10.1021/acs.jpca.0c05677
J. Phys. Chem. A XXXX, XXX, XXX−XXX

inclusion of a better extrapolation of the $CO_2 + C \leftrightarrow CO + CO$ reaction. Fourthly, the assumption of the full efficiency of vibrational energy conversion into lowering the activation energy could impact the results presented in this work. This step also includes a better assessment of the electronically excited states of O, CO, and O_2, which may enhance the forward or backward reactions. See Fox and Hác's review[68] for a discussion on the role of excited O atoms in the redistribution of energy, and the work of Morillo-Candas et al.[66] hints at the role of electronically excited CO that enhances recombination by collisions with O_2 molecules, which if excited may also be important for recombination as the work of Sharipov[64] suggests. Fifthly, the separability of the modes is a key shortcoming of this model and this should be addressed in the future. Sixthly, and as a consequence of assuming mode separability, there are a series of accidental resonances, which might redistribute the energy between the vibrational modes of CO_2. A simple way to include these processes is to apply a simplified Landau−Teller model to yield an additional set of near-resonant rates and deploy these in our model, according to the expression found in refs 31, 91, and 92. Finally, the radiative losses in a CO_2 gas may be modeled through the inclusion of vibrational Einstein coefficients such as those presented in ref 93. Although this is not as straightforward as presented here, due to the use of "extreme states" in this work, some sort of binning or lumping of radiative processes could achieve the desired outcome.

With 20,000+ rates, that the presented model is not tractable for more than a 0D/1D treatment. The use of this model (and eventual future versions) in higher-order problems requires the use of a reduced-order model to decrease the complexity and computational overhead. Two approaches known to the authors are binning[7,94,95] and Fokker−Planck methods,[96−99] which have already been applied to CO_2 SSH models and proven to be more computationally efficient than their state-to-state counterparts. The application of one of these models is of paramount importance when dealing with 2D or 3D geometries.

Concluding Remarks. This work aimed at furthering the state-of-the-art on CO_2 vibrationally specific kinetics by implementing improved theoretical approaches, including a better description of the ground and excited electronic levels manifold, improved state-specific collisional models such as the forced harmonic oscillator theory—which has been extended to triatomic molecules such as CO_2—and compiling a set of adequate chemistry rates, yielding a self-contained model capable of making predictive simulations of CO_2 dissociation processes in shocked flows. However, in a certain sense, a completely adequate modeling of CO_2 state-to-state processes is an endeavor still out of reach, which will require extensive theoretical and experimental work, with the application of novel approaches even further beyond the state-of-the-art of our model. We hope that this work may inspire other authors to take further steps in this direction. The state-to-state rate coefficients, computed or adapted for this work, are publicly made available as part of the STELLAR database.[100] Additionally, the codes used to generate the state-specific rates of CO_2 are also made available in the same address as the STELLAR database.

AUTHOR INFORMATION

Corresponding Author

João Vargas − *Instituto de Plasmas e Fusão Nuclear, Instituto Superior Técnico, Universidade de Lisboa, Lisboa 1049-001, Portugal;* orcid.org/0000-0002-5909-1512; Email: joao.f.vargas@tecnico.ulisboa.pt

Authors

Bruno Lopez − *Department of Aerospace Engineering, University of Illinois at Urbana−Champaign, Urbana, Illinois 61801, United States*

⊗**Mário Lino da Silva** − *Instituto de Plasmas e Fusão Nuclear, Instituto Superior Técnico, Universidade de Lisboa, Lisboa 1049-001, Portugal*

Complete contact information is available at: https://pubs.acs.org/10.1021/acs.jpca.0c05677

Notes

The authors declare no competing financial interest.

⊗Email: mlinodasilva@tecnico.ulisboa.pt

ACKNOWLEDGMENTS

The authors thank Xinchuan Huang for sharing the coefficients for the NASA-Ames-2 PES of CO_2. Additionally, the authors would like to thank the following colleagues for the many discussions and exchanges over the course of this work: Brett Cruden for providing insight on his macroscopic rates review, as well as information on the recent NASA CO_2 shock-tube campaigns; Vasco Guerra and Tiago Silva for useful discussions on CO_2 plasma reforming, state-to-state kinetics, and the $T_{v_1} = T_{v_2}$ approximation; Élio Pereira for useful discussions on VE transitions; Elena Kustova and Mariia Mekhonoshina for useful discussions on CO_2 state-to-state modeling; Jonathan Tennyson for discussions on vibrational chaos; Theresa Urbanietz for insight on the postprocessing of FTIR experiments of refs 22 and 23; Amal Sahai for discussions on the state-to-state binning theory; and Pedro Viegas for insight on the Fokker−Planck theory. The authors would like to thank the reviewers for useful comments that helped improving the quality of the manuscript. Finally, a heartfelt acknowledgment to Marco Panesi who hosted J. Vargas at the University of Illinois at Urbana−Champaign for a year as a visiting scholar and without whom this work would not have been possible. This work has been partially supported by the Portuguese FCT, under Projects UIDB/50010/2020 and UIDP/50010/2020 and the grants PD/BD/114325/2016 (PD-F APPLAuSE) and by the European Space Agency, under grant 4000118059/16/NL/KML/FG "standard kinetic models for CO_2 dissociating flows".

ADDITIONAL NOTES

[a]Excluding perturbations from other states.
[b]Unless the translational temperature is very high.

REFERENCES

(1) Bongers, W.; Bouwmeester, H.; Wolf, B.; Peeters, F.; Welzel, S.; van den Bekerom, D.; den Harder, N.; Goede, A.; Graswinckel, M.; Groen, P. W.; et al. Plasma-driven dissociation of CO_2 for fuel synthesis. *Plasma Process. Polym.* **2017**, *14*, No. 1600126.

(2) Bogaerts, A.; Tu, X.; van Rooij, G. J.; van de Sanden, M. C. M. In *Carbon Dioxide Utilization: From Fundamentals to Production Processes*; North, M., Styring, P., Eds.; De Gruyter: Berlin, Germany, 2019; Chapter 28, Vol. 2, pp 585−634.

(3) Guerra, V.; Silva, T.; Ogloblina, P.; Grofulović, M.; Terraz, L.; Lino da Silva, M.; Pintassilgo, C. D.; Alves, L. L.; Guaitella, O. The case for in situ resource utilisation for oxygen production on Mars by non-equilibrium plasmas. *Plasma Sources Sci. Technol.* **2017**, *26*, No. 11LT01.

(4) Armenise, I.; Kustova, E. V. State-to-state models for CO_2 molecules: From the theory to an application to hypersonic boundary layers. *Chem. Phys.* **2013**, *415*, 269−281.

(5) Kustova, E.; Nagnibeda, E.; Armenise, I. Vibrational-Chemical Kinetics in Mars Entry Problems. *Open Plasma Phys. J.* **2014**, *7*, 76−87.
(6) Heijkers, S.; Snoeckx, R.; Kozák, T.; Silva, T.; Godfroid, T.; Britun, N.; Snyders, R.; Bogaerts, A. CO_2 conversion in a microwave plasma reactor in the presence of N_2: Elucidating the role of vibrational levels. *J. Phys. Chem. C* **2015**, *119*, 12815−12828.
(7) Sahai, A. Reduced-Order Modeling of Non-Boltzmann Thermochemistry and Radiation for Hypersonic Flows. Ph.D. thesis, University of Illinois at Urbana-Champaign, 2019.
(8) Terraz, L.; Silva, T.; Morillo-Candas, A. S.; Guaitella, O.; Tejero-del Caz, A.; Alves, L. L.; Guerra, V. Influence of N_2 on the CO_2 vibrational distribution function and dissociation yield in non-equilibrium plasmas. *J. Phys. D: Appl. Phys.* **2019**, *53*, No. 094002.
(9) Treanor, C. E. Vibrational Energy Transfer in High-Energy Collisions. *J. Chem. Phys.* **1965**, *43*, 532−538.
(10) Zelechow, A.; Rapp, D.; Sharp, T. E. Vibrational-Vibrational-Translational Energy Transfer between Two Diatomic Molecules. *J. Chem. Phys.* **1968**, *49*, 286−299.
(11) Adamovich, I. V.; Macheret, S. O.; Rich, J. W.; Treanor, C. E. Vibrational relaxation and dissociation behind shock waves part 1: Kinetic Rate Models. *AIAA J.* **1995**, *33*, 1064−1069.
(12) Adamovich, I. V.; Macheret, S. O.; Rich, J. W.; Treanor, C. E. Vibrational Relaxation and Dissociation behind Shock Waves Part 2: Master Equation Modeling. *AIAA J.* **1995**, *33*, 1070−1075.
(13) Adamovich, I. V.; Macheret, S. O.; Rich, J. W.; Treanor, C. E. Vibrational energy transfer rates using a Forced Harmonic Oscillator model. *J. Thermophys. Heat Transfer* **1998**, *12*, 57−65.
(14) Macheret, S. O.; Adamovich, I. V. Semiclassical modeling of state-specific dissociation rates in diatomic gases. *J. Chem. Phys.* **2000**, *113*, 7351−7361.
(15) Lino da Silva, M.; Guerra, V.; Loureiro, J. State-resolved dissociation rates for extremely nonequilibrium atmospheric entries. *J. Thermophys. Heat Transfer* **2007**, *21*, 40−49.
(16) Cruden, B. A.; Brandis, A. M.; Macdonald, M. E. In *Characterization of CO Thermochemistry in Incident Shockwaves*, 2018 Joint Thermophysics and Heat Transfer Conference, 2018; pp 1−22.
(17) Kozák, T.; Bogaerts, A. Evaluation of the energy efficiency of CO_2 conversion in microwave discharges using a reaction kinetics model. *Plasma Sources Sci. Technol.* **2015**, *24*, No. 015024.
(18) Rosser, W. A.; Hoag, E.; Gerry, E. T. Relaxation of excess populations in the lower laser level $CO_2(100)$. *J. Chem. Phys.* **1972**, *57*, 4153−4164.
(19) Losev, S. A. Kinetics of vibrational energy transfer in carbon dioxide and its mixtures with other gases. *Combust., Explos. Shock Waves* **1976**, *12*, 141−179.
(20) Allen, D. C.; Scragg, T.; Simpson, C. J. Low temperature fluorescence studies of the deactivation of the bend−stretch manifold of CO_2. *Chem. Phys.* **1980**, *51*, 279−298.
(21) Millot, G.; Roche, C. State-to-state vibrational and rotational energy transfer in CO_2 gas from time-resolved raman−infrared double resonance experiments. *J. Raman Spectrosc.* **1998**, *29*, 313−320.
(22) Urbanietz, T.; Böke, M.; Schulz-von der Gathen, V.; Von Keudell, A. Non-equilibrium excitation of CO_2 in an atmospheric pressure helium plasma jet. *J. Phys. D: Appl. Phys.* **2018**, *51*, No. 345202.
(23) Stewig, C.; Schüttler, S.; Urbanietz, T.; Boeke, M.; von Keudell, A. Excitation and dissociation of CO_2 heavily diluted in noble gas atmospheric pressure plasma. *J. Phys. D: Appl. Phys.* **2020**, *53*, No. 125205.
(24) Lino da Silva, M.; Guerra, V.; Loureiro, J.; Sá, P. A. Vibrational distributions in N_2 with an improved calculation of energy levels using the RKR method. *Chem. Phys.* **2008**, *348*, 187−194.
(25) Huang, X.; Schwenke, D. W.; Tashkun, S. A.; Lee, T. J. An isotopic-independent highly accurate potential energy surface for CO_2 isotopologues and an initial $^{12}C^{16}O_2$ infrared line list. *J. Chem. Phys.* **2012**, *136*, No. 124311.
(26) Hulburt, H. M.; Hirschfelder, J. O. Potential energy functions for diatomic molecules. *J. Chem. Phys.* **1941**, *9*, 61−69.
(27) Quapp, W.; Winnewisser, B. P. What you thought you already knew about the bending motion of triatomic molecules. *J. Math. Chem.* **1993**, *14*, 259−285.
(28) Chedin, A. The carbon dioxide molecule. Potential, spectroscopic, and molecular constants from its infrared spectrum. *J. Mol. Spectrosc.* **1979**, *76*, 430−491.
(29) Grebenshchikov, S. Y. Infrared spectra of neutral bent carbon dioxide. *J. Phys. Chem. A* **2017**, *121*, 4296−4305.
(30) Hwang, D. Y.; Mebel, A. M. Ab initio study of spin-forbidden unimolecular decomposition of carbon dioxide. *Chem. Phys.* **2000**, *256*, 169−176.
(31) Lino da Silva, M.; Vargas, J.; Loureiro, J. *STELLAR CO_2 Version 2: A Database for Vibrationally-Specific Excitation and Dissociation Rates for Carbon Dioxide*, 2018, pp 1−30. Available at: http://esther.ist.utl.pt/stellar/STELLAR-CO2-report.pdf.
(32) Kerner, E. H. Note on the Forced and Damped Oscillator in Quantum Mechanics. *Can. J. Phys.* **1958**, *36*, 371−377.
(33) Nikitin, E. E.; Osipov, A. I. Vibrational Relaxation in Gases, In *Kinetic and Catalysis*, VINITI, All-Union Institute of Scientific and Technical Information, Moscow1977; Vol. *4*, Chap. 2.
(34) Lino da Silva, M.; Guerra, V.; Loureiro, J. Nonequilibrium dissociation processes in hyperbolic atmospheric entries. *J. Thermophys. Heat Transfer* **2007**, *21*, 303−310.
(35) Lino da Silva, M.; Guerra, V.; Loureiro, J. State-resolved dissociation rates for extremely nonequilibrium atmospheric entries. *J. Thermophys. Heat Transfer* **2007**, *21*, 40−49.
(36) Lino da Silva, M.; Loureiro, J.; Guerra, V. A multiquantum dataset for vibrational excitation and dissociation in high-temperature O 2-O 2 collisions. *Chem. Phys. Lett.* **2012**, *531*, 28−33.
(37) Lino da Silva, M.; Lopez, B.; Guerra, V.; Loureiro, J. In *A Multiquantum State-to-State Model for the Fundamental States of Air: The Stellar Database*, Proceedings of 5th International Workshop Radiation of High Temperature Gases in Atmospheric Entry,Ouwehand, L., Ed.; ESASP, 2012; Vol. *714*, p 16.
(38) Lopez, B.; Lino da Silva, M. In *Non-Boltzmann Analysis of Hypersonic Air Re-Entry Flows*. 11th AIAA/ASME Joint Thermophysics and Heat Transfer Conference, 2014, pp 1−19.
(39) Le Roy, R. J.; Huang, Y.; Jary, C. An accurate analytic potential function for ground-state N_2 from a direct-potential-fit analysis of spectroscopic data. *J. Chem. Phys.* **2006**, *125*, No. 164310.
(40) Cottrell, T. L.; Ream, N. Transition probability in molecular encounters. Part 2.-Vibrational relaxation time in methane. *Trans. Faraday Soc.* **1955**, *51*, 1453−1465.
(41) Jaffe, R. *Vibrational and Rotational Excitation and Dissociation of CO_2 Reexamined*, AIAA paper 2011-447, 49th AIAA Aerospace Sciences Meeting including the New Horizons Forum and Aerospace Exposition, Orlando, Florida, 2011; pp 1−14.
(42) Xu, L. T.; Jaffe, R. L.; Schwenke, D. W.; Panesi, M. *The Effect of the Spin-Forbidden $CO(^1\Sigma^+) + O(^3P) \rightarrow CO_2(^1\Sigma_g^+)$ Recombination Reaction on Afterbody Heating of Mars Entry Vehicles*, AIAA paper 2017-3486, 47th AIAA Thermophysics Conference, 2017; pp 1−21.
(43) Nikitin, E. E. Nonadiabatic transitions: What we learned from the old masters and how much we owe them. *Annu. Rev. Phys. Chem.* **1999**, *50*, 1−21.
(44) Bondybey, V. E.; Miller, T. A. Radiative and radiationless vibronic deactivation rates in selectively excited CO+. *J. Chem. Phys.* **1978**, *69*, 3597−3602.
(45) Katayama, D. H.; Miller, T. A.; Bondybey, V. E. Radiative decay and radiationless deactivation in selectively excited CN. *J. Chem. Phys.* **1979**, *71*, 1662−1669.
(46) Katayama, D. H.; Welsh, J. A. The effect of isotopic substitution on the collisional quenching of vibronically excited CO+. *J. Chem. Phys.* **1983**, *79*, 3627−3632.
(47) Katayama, D. H.; Welsh, J. A. The effect of temperature on the collisional deactivation of electronically excited CO+. *Chem. Phys. Lett.* **1984**, *106*, 74−78.
(48) Dentamaro, A. V.; Katayama, D. H. Collision induced transitions between the $A^2\Pi_i(v = 0)$ and $X^2\Sigma^+(v = 10)$ states of CO+. *J. Chem. Phys.* **1989**, *90*, 91−95.

https://dx.doi.org/10.1021/acs.jpca.0c05677
J. Phys. Chem. A XXXX, XXX, XXX−XXX

(49) Bachmann, R.; Li, X.; Ottinger, C.; Vilesov, A. F. Molecular-beam study of the collisional intramolecular coupling of $N_2(B^3\Pi_g)$ with the $N_2(A^3\Sigma_u^+)$ and $N_2(W^3\Delta_u)$ states. *J. Chem. Phys.* **1992**, *96*, 5151−5164.
(50) Jihua, G.; Ali, A.; Dagdigian, P. J. State-to-state collisional interelectronic and intraelectronic energy transfer involving CN $A^2\Pi$ v=3 and $^2\Sigma^+$ v=7 rotational levels. *J. Chem. Phys.* **1986**, *85*, 7098−7105.
(51) Piper, L. G. State-to-state $N_2(A^3\Sigma_u^+)$ energy pooling reactions. II. The formation and quenching of N2($B\ ^3\Pi_g$, v′=1-12). *J. Chem. Phys.* **1988**, *88*, 6911−6921.
(52) Clark, T. C.; Garnett, S. H.; Kistiakowsky, G. B. Exchange Reaction of ^{18}O Atoms with CO_2 and with SO_2 in Shock Waves. *J. Chem. Phys.* **1970**, *52*, 4692−4698.
(53) Park, C.; Howe, J. T.; Jaffe, R. L.; Candler, G. V. Review of chemical-kinetic problems of future NASA missions, II: Mars entries. *J. Thermophys. Heat Transfer* **1994**, *8*, 9−23.
(54) Annaloro, J. Modèles collisionels-radiatifs appliqués aux situations d'entrée atmosphérique martienne et terrestre. Ph.D. Thesis, University of Rouen, 2013.
(55) Macheret, S.; Losev, S.; Chernyĭ, G.; Potapkin, B. *Physical and Chemical Processes in Gas Dynamics: Cross Sections and Rate Constants for Physical and Chemical Processes, Volume I*; American Institute of Aeronautics and Astronautics, 2002; Vol. *196*.
(56) Chernyĭ, G.; Losev, S.; Macheret, S.; Potapkin, B. *Physical and Chemical Processes in Gas Dynamics: Physical and Chemical Kinetics and thermodynamics of Gases and Plasmas, Volume II*; American Institute of Aeronautics and Astronautics, 2002; Vol. *196*.
(57) Fridman, A. *Plasma Chemistry*; Cambridge University Press, 2008; pp 1−978.
(58) Kustova, E.; Savelev, A.; Armenise, I. State-Resolved Dissociation and Exchange Reactions in CO2 Flows. *J. Phys. Chem. A* **2019**, *123*, 10529−10542.
(59) Sulzmann, K. G. P.; Myers, B. F.; Bartle, E. R. CO oxidation. I. Induction period preceding CO_2 formation in shock-heated CO−O_2−Ar mixtures. *J. Chem. Phys.* **1965**, *42*, 3969−3979.
(60) Thielen, K.; Roth, P. Stoßtwellenuntersuchungen zum Start der Reaktion CO + O_2. *Ber. Bunsen-Ges. Phys. Chem.* **1983**, *87*, 920−925.
(61) Kwak, H. S.; Uhm, H. S.; Hong, Y. C.; Choi, E. H. Disintegration of Carbon Dioxide Molecules in a Microwave Plasma Torch. *Sci. Rep.* **2015**, *5*, No. 18436.
(62) Schofield, K. An evaluation of kinetic rate data for reactions of neutrals of atmospheric interest. *Planet. Space Sci.* **1967**, *15*, 643−664.
(63) Ibragimova, L. B. Recommended rate constants of CO + O_2 reversible CO_2 + O reactions. *Khim. Fiz.* **1991**, *10*, 307−310.
(64) Sharipov, A. S.; Starik, A. M. Theoretical study of the reaction of carbon monoxide with oxygen molecules in the ground triplet and singlet delta states. *J. Phys. Chem. A* **2011**, *115*, 1795−1803.
(65) Varga, T. Optimization and Uncertainty Quantification of Hydrogen and Syngas Combustion Models. Ph.D. Thesis, Eötvös Loránd University, 2017.
(66) Morillo-Candas, A. S.; Guerra, V.; Guaitella, O. Time Evolution of the Dissociation Fraction in rf CO_2 Plasmas: Impact and Nature of Back-Reaction Mechanisms. *J. Phys. Chem. C* **2020**, *124*, 17459−17475.
(67) Husain, D.; Young, A. N. Kinetic investigation of ground state Carbon Atoms, C(2^3P_j). *J. Chem. Soc., Faraday Trans. 2* **1975**, *71*, 525−531.
(68) Fox, J. L.; Haćˊ, A. B. Escape of O(^{3}P), O(^{1}D), and O(^{1}S) from the Martian atmosphere. *Icarus* **2018**, *300*, 411−439.
(69) Dunlea, E. J.; Ravishankara, A. R. Kinetic studies of the reactions of O(^{1}D) with several atmospheric molecules. *Phys. Chem. Chem. Phys.* **2004**, *6*, 2152−2161.
(70) Yee, J. H.; Guberman, S. L.; Dalgarno, A. Collisional quenching of O(^{1}D) by O(^{3}P). *Planet. Space Sci.* **1990**, *38*, 647−652.
(71) Wine, P. H.; Ravishankara, A. R. Kinetics of O(^{1}D) interactions with the atmospheric gases N_2, N_2O, H_2O, H_2, CO_2, and O_3. *Chem. Phys. Lett.* **1981**, *77*, 103−109.
(72) Donovan, R. J.; Husain, D. Recent advances in the chemistry of electronically excited atoms. *Chem. Rev.* **1970**, *70*, 489−516.
(73) Davidson, J. A.; Sadowski, C. M.; Schiff, H. I.; Streit, G. E.; Howard, C. J.; Jennings, D. A.; Schmeltekopf, A. L. Absolute rate constant determinations for the deactivation of O(^{1}D) by time resolved decay of O(^{1}D)-O(^{3}P) emission. *J. Chem. Phys.* **1976**, *64*, 57.
(74) Hanson, R. K. Shock-tube study of carbon monoxide dissociation kinetics. *J. Chem. Phys.* **1974**, *60*, 4970−4976.
(75) Fairbairn, A. R. The dissociation of carbon monoxide. *Proc. R. Soc.* **1969**, *312*, 207−227.
(76) Warnatz, J. In *Combustion Chemistry*; Gardiner, W. C., Ed.; Springer: New York, NY, 1984; pp 197−360.
(77) Park, C. *Nonequilibrium Hypersonic Aerothermodynamics*; John Wiley & Sons, 1989.
(78) Teulet, P.; Gonzalez, J. J.; Mercado-Cabrera, A.; Cressault, Y.; Gleizes, A. One-dimensional hydro-kinetic modelling of the decaying arc in air-PA66-copper mixtures: II. Study of the interruption ability. *J. Phys. D: Appl. Phys.* **2009**, *42*, No. 185207.
(79) Park, C. Review of chemical-kinetic problems of future NASA missions, I: Earth entries. *J. Thermophys. Heat Transfer* **1993**, *7*, 385−398.
(80) Billing, G. D. Semiclassical calculation of energy transfer in polyatomic molecules I. the N_2+CO_2 system. *Chem. Phys.* **1979**, *41*, 11−20.
(81) Billing, G. D. Semiclassical calculation of energy transfer in polyatomic molecules VI. On the theory for linear triatomic molecules. *Chem. Phys.* **1981**, *61*, 415−430.
(82) Sharma, R. D.; Brau, C. A. Energy transfer in near-resonant molecular collisions due to long-range forces with application to transfer of vibrational energy from v_3 mode of CO_2 to N_2. *J. Chem. Phys.* **1969**, *50*, 924−930.
(83) Wolf, A. J.; Peeters, F. J. J.; Groen, P. W. C.; Bongers, W. A.; van de Sanden, M. C. M. CO_2 Conversion in Nonuniform Discharges: Disentangling Dissociation and Recombination Mechanisms. *J. Phys. Chem. C* **2020**, *124*, 16806−16819.
(84) Anokhin, E. M. Physical and Chemical Relaxation Behind Strong Shock Waves in CO_2−N_2 Mixtures. Ph.D. Thesis, Moscow Institute of Physics and Technology (MIPT), 2005.
(85) Chikhaoui, A.; Lino da Silva, M.; Mota, S.; Resendes, D. Support during the MIPT Shock Tube Calibration, 2008, pp 1−49.
(86) Beck, J. *CFD Validation in a CO_2 Environment: Synthesis Report, Technical Report, Fluid Gravity*; Engineering, 2008.
(87) Reynier, P.; Bugel, M.; Smith, A. Survey of European and major ISC facilities for supporting Mars and sample return mission aerothermodynamics and tests required for thermal protection system and dynamic stability. *Int. J. Aerosp. Eng.* **2011**, *2011*, No. 937629.
(88) Anokhin, E. M.; Ivanova, T. Y.; Kudryavtsev, N. N.; Starikovskii, A. Y. Dynamics of radiation in a CO:N_2 mixture behind strong shock waves. *High Temp.* **2007**, *45*, 733−739.
(89) Anokhin, E.; Ivanova, T.; Koudriavtsev, N.; Starikovskii, A. *Energy Spectral Distribution behind Strong Shock Waves in CO:N_2 Mixture*, AIAA paper 2007-814, 45th AIAA Aerospace Sciences Meeting and Exhibit, Reno, Nevada, 2007.
(90) Reynier, P. Survey of CO_2 radiation experimental data, **2020**, arXiv preprint, arXiv:2007.04869.
(91) Landau, L. D. On the Theory of Sound Dispersion. In *Collected Papers of L.D. Landau*; Ter Haar, D., Ed.; Pergamon: Moscow, 1965; pp 147−153.
(92) Nevdakh, V. V.; Orlov, L. N.; Leshenyuk, N. S. Temperature dependence of the vibrational relaxation rate constants of CO_2 (00^01) in binary mixtures. *J. Appl. Spectrosc.* **2003**, *70*, 276−284.
(93) Vargas, J.; Lopez, B.; Lino da Silva, M. CDSDv: A compact database for the modeling of high-temperature CO_2 radiation. *J. Quant. Spectrosc. Radiat. Transfer* **2020**, *245*, No. 106848.
(94) Liu, Y.; Panesi, M.; Sahai, A.; Vinokur, M. General multi-group macroscopic modeling for thermo-chemical non-equilibrium gas mixtures. *J. Chem. Phys.* **2015**, *142*, No. 134109.
(95) Sahai, A.; Johnston, C. O.; Lopez, B.; Panesi, M. Flow-radiation coupling in CO_2 hypersonic wakes using reduced-order non-Boltzmann models. *Phys. Rev. Fluids* **2019**, *4*, No. 093401.
(96) Diomede, P.; Van De Sanden, M. C.; Longo, S. Insight into CO_2 dissociation in plasma from numerical solution of a vibrational diffusion equation. *J. Phys. Chem. C* **2017**, *121*, 19568−19576.

https://dx.doi.org/10.1021/acs.jpca.0c05677
J. Phys. Chem. A XXXX, XXX, XXX−XXX

(97) Diomede, P.; Van De Sanden, M. C.; Longo, S. Vibrational kinetics in plasma as a functional problem: A flux-matching approach. *J. Phys. Chem. A* **2018**, *122*, 7918−7923.
(98) Longo, S.; van de Sanden, M. C.; Diomede, P. Fokker−Planck equation for chemical reactions in plasmas. *Rend. Lincei Sci. Fis. Nat.* **2019**, *30*, 25−30.
(99) Viegas, P.; Van de Sanden, M. C.; Longo, S.; Diomede, P. Validation of the Fokker-Planck approach to vibrational kinetics in CO_2 plasma. *J. Phys. Chem. C* **2019**, *123*, 22823−22831.
(100) STELLAR Database. http://esther.ist.utl.pt/pages/stellar.html (accessed July 2020).

https://dx.doi.org/10.1021/acs.jpca.0c05677
J. Phys. Chem. A XXXX, XXX, XXX−XXX